

Seismic fragility of buried steel natural gas pipelines due to axial compression at geotechnical discontinuities

Grigorios Tsinidis¹, Luigi Di Sarno², Anastasios Sextos³, and Peter Furtner⁴

¹ Vienna Consulting Engineers ZT GmbH, Austria & University of Sannio, Italy

² University of Liverpool, United Kingdom & University of Sannio, Italy

³ University of Bristol, United Kingdom

⁴ Vienna Consulting Engineers ZT GmbH, Austria

Corresponding Author: Grigorios Tsinidis, University of Sannio, School of Engineering, Piazza Roma, 21, 82100, Benevento, Italy, email: tsinidis.grigorios@gmail.com

Abstract: This paper presents an extended set of numerical fragility functions for the structural assessment of buried steel natural gas (NG) pipelines subjected to axial compression caused by transient seismic ground deformations. The study focuses on NG pipelines crossing sites with a vertical geotechnical discontinuity, where high compression straining of a buried pipeline is expected to occur under seismic transient ground deformations. A de-coupled numerical framework is developed for this purpose, which includes a 3D finite element model of the pipe-trench system employed to evaluate rigorously the soil-pipe interaction effects on the pipeline axial response in a quasi-static manner. One-dimensional soil response analyses are used to determine critical ground deformation patterns at the vicinity of the geotechnical discontinuity, caused by the ground shaking. A comprehensive parametric analysis is performed by implementing the proposed analytical framework for an ensemble of 40 recorded earthquake ground motions. Crucial parameters that affect the seismic response and therefore the seismic vulnerability of buried steel NG pipelines namely, the diameter, wall thickness, burial depth and internal pressure of the pipeline, the backfill compaction level, the pipe-soil interface friction characteristics, the soil deposits characteristics, as well as initial geometric imperfections of the walls of the pipeline, are systematically considered. The analytical fragility functions are developed in terms of peak ground velocity (*PGV*) at the ground surface, for four performance limit states, considering all the associated uncertainties. The study contributes towards a reliable quantitative risk assessment of buried steel NG pipelines, crossing similar sites, subjected to seismically-induced transient ground deformations.

Keywords: *natural gas pipelines; seismic response; fragility curves; soil-pipe interaction; transient ground deformations; steel pipelines; local buckling*

1. Introduction

Earthquake-induced damage on Natural Gas (NG) pipeline networks may lead to significant downtimes, which in turn may result in high direct and indirect economic losses. The 1999 Chi-Chi earthquake in Taiwan, for instance, caused noticeable damage on natural gas supply systems, with the associated economic loss for the major natural gas companies exceeding \$25

1 million (Chen et al. 2000; Lee et al. 2009) More importantly, severe damages may trigger
2 ignition or explosions with life-treating consequences and significant effects on the
3 environment. The 1995 Hyogo-Ken Nambu earthquake in Japan is a rather devastating
4 example since the particular earthquake caused gas leakages from buried pipelines at 234
5 different locations, which subsequently led to more than 530 fires (EQE 1995; Scawthorn et al.
6 1995). The above aspects highlight the importance of simple, yet efficient, methods for
7 structural vulnerability assessment of NG pipeline networks.

8 Buried steel NG pipelines are found to be quite vulnerable to high strain imposed by permanent
9 ground deformations, associated with seismically-induced ground failures, i.e. fault
10 movements, landslides, liquefaction-induced settlements or uplifting and lateral spreading
11 (O'Rourke M.J. and Liu 1999; Sarvanis et al. 2018; Lanzano et al. 2015; Karamitros et al.
12 2007; 2016; Vazouras et al. 2010; 2012; Vazouras and Karamanos 2017; Melissianos et al.
13 2017a, b, c; Sarvanis et al. 2018; Demirci et al. 2018; Tsatsis et al. 2018). Although to a lesser
14 extent, transient ground deformations, induced by seismic wave propagation, have also
15 contributed to seismic damage of steel pipelines (Housner and Jennings 1972; O'Rourke T.D.
16 and Palmer 1994; O'Rourke M.J. 2009). Indeed, transient ground deformation may trigger
17 diverse damage modes on continuous NG pipelines, including (i) shell-mode or local buckling,
18 (ii) beam-mode buckling, (iii) pure tensile rupture, (iv) flexural bending failure and (v)
19 excessive ovaling deformation of the section (O'Rourke M.J. and Liu 1999). Recent studies
20 have demonstrated that pipelines embedded in heterogeneous sites and/or subjected to
21 asynchronous ground seismic motions are likely to be further affected by appreciable
22 deformations and strains due to transient ground deformations, which in turn may lead to
23 buckling damages on the pipeline (Psyrras and Sextos 2018; Psyrras et al. 2019).

24 In practice, the seismic risk assessment of pipelines is mainly performed, by implementing
25 empirical fragility relations, which were constructed on the basis of observations of the
26 behaviour of buried pipelines during past earthquakes (e.g. ALA 2001; NIBS 2004; Gehl et al.
27 2014). A detailed review of available empirical relations may be found in Tsinidis et al.
28 (2019a). These relations normally provide correlations between the pipeline *repair rate*, *RR*,
29 i.e. the number of pipe repairs per unit of pipeline length, and a selected seismic *intensity*
30 *measure*, expressing the seismic intensity.

31 The majority of available fragility relations refer to cast-iron or asbestos cement segmented
32 pipelines, the seismic response of which is quite distinct compared to continuous pipelines,
33 such as buried NG pipelines (O'Rourke M.J. and Liu 1999). The lack of relevant damage
34 reports and therefore of relevant fragility relations for continuous pipelines has been attributed
35 by some researchers to their better performance, compared to the segmental pipelines, when
36 subjected to seismically-induced transient ground deformations. However, as stated above,
37 under certain conditions, transient ground deformations may impose significant strains on
38 buried pipelines.

39 The implementation of *repair rate* as an engineering demand parameter (EDP) does not
40 provide detailed information regarding the severity of damage, as well as the type of required
41 repair, while the accuracy of the repair reports that constitute the basis for the development of
42 empirical fragility functions may be debatable, since these are commonly drafted after a short

period from the main event and under the pressure for rapid restorations. Moreover, available empirical relations were developed on the basis of damage reports on pipeline networks found in USA and Japan, whilst in southern Europe or other seismic prone areas there is an evident lack of relevant information. Evidently, the applicability of the empirical fragility relations is restricted to cases where the network characteristics, e.g. pipe dimensions and materials, soil conditions etc, and the ground motion characteristics, are similar to the relevant characteristics of the sample used to develop the relations. Finally, available fragility relations do not disaggregate between distinct damage modes and associated effects on the structural integrity and serviceability of the pipeline. Along these lines, a general and unconditional use of these relations might introduce a degree of uncertainty in the seismic risk assessment of networks with distinct characteristics (Psyrras and Sextos 2018).

A limited number of numerical fragility curves that compute probabilities of failure for well-defined limit states in the ‘classical sense’ have been proposed, recently (Lee et al. 2016; Jahangiri and Shakid 2018). However, available numerical fragility functions refer to rather limited number soil-pipe configurations and do not cover NG pipelines with diameters larger than 800 mm that are commonly used in transmission NG networks. More importantly, the relevant numerical studies do not examine thoroughly salient parameters that may affect the response and hence the vulnerability of buried NG pipelines under seismically-induced transient ground deformations, such as the effects of the internal operational pressure of the pipeline or the initial geometric imperfection of the walls of the pipes and the spatial variability of soil conditions.

In the light of the above considerations and knowledge gaps, this paper presents an extended set of numerical fragility curves for the structural assessment of buried steel NG pipelines subjected to axial compression caused by transient seismic ground deformations. The study focuses on pipelines crossing perpendicularly a vertical geotechnical discontinuity with an abrupt change on the soil properties, where the potential of high compression strain and therefore buckling failures is expected to be increased under seismic transient ground deformations. A detailed analytical framework is developed for this purpose, which is employed in a comprehensive parametric analysis of large number of pipe-soil configurations and for an ensemble of 40 recorded earthquake ground motions. Crucial parameters affecting the response of buried steel pipelines namely the diameter, wall thickness, burial depth and internal pressure of the pipeline, the existence of initial geometric wall imperfections of the pipeline, the trench soil compaction level, the pipe-backfill interface friction characteristics and the variability of the characteristics of the soil deposits, are thoroughly accounted for in the study. The analytical fragility curves are developed in terms of peak ground velocity (*PGV*) at the ground surface, for four performance limit states, considering the associated uncertainties.

2. Definition of problem

Fig. 1 illustrates schematically the problem examined herein. A continuous buried steel NG pipeline of external diameter D and wall thickness t is embedded in a surficial block of soil at a burial depth h . The surficial block of soil is resting over a soil deposit with a vertical geotechnical discontinuity. The latter divides the deposit into two subdeposits, i.e. subdeposit 1

and subdeposit 2, with abrupt changes on their physical and mechanical properties. The total depth of the soil deposit is H . It is noted that the selected soil deposits constitute idealized cases to facilitate the numerical parametric study presented herein. The soil-pipe system is subjected to ground seismic shaking, in the form of upward propagated, vertically polarized plane shear waves, which causes a dissimilar ground movement of the adjusted subdeposits. The dissimilar ground movement of the adjusted soil subdeposits produces a differential horizontal ground deformation along the pipeline axis near the critical section of the geotechnical discontinuity, which subsequently is transferred via the pipe-trench soil interface on the pipeline causing its compressive-tensional axial straining. A potential high axial compression strain of the pipeline might finally lead to a failure of the pipeline in the form of local buckling. Based on the above considerations, a numerical framework is developed to evaluate the vulnerability of the embedded steel NG pipeline under an ensemble of carefully selected real records.

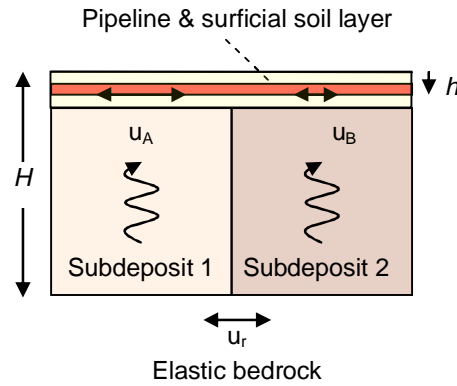


Fig. 1 Schematic view of the examined problem (H : depth of the soil deposit, h : burial depth of the pipeline, u_r : seismic displacement at bedrock, u_A and u_B : horizontal seismic deformations of the adjacent soil subdeposits).

3. Analytical framework

3.1 General flowchart

The extended dimensions of the problem in hand, the need for refined meshes to capture potential buckling failure of the pipeline, the complexity in simulating the material and geometrical nonlinearities, i.e. sliding and/or detachment phenomena at the soil-pipe interface, during ground shaking, the uncertainty in the definition of the characteristics of heterogeneous soil sites, and issues associated with proper selection of seismic ground motions, are all reasons that render a fully 3D time history analysis of the coupled pipeline-trench soil system computationally prohibitive (Psyrras and Sextos 2018).

Generally, the inertial soil-structure interaction (SSI) effects are not considered to be a key factor in the context of the dynamic soil-pipe interaction (SPI) problem mainly due to the reduced mass of the pipe in comparison to that of the soil (O'Rourke M.J. and Hmadi 1988). This allows for a decoupling of the problem in successive stages in order to reduce the high computational cost, associated with a fully-fledged 3D SPI dynamic analysis. Moreover, it allows for the investigation of the effect of transient ground deformation on the response of the embedded pipeline in a quasi-static manner.

Based on the above considerations, an analytical framework was developed within this study to evaluate thoroughly the seismic vulnerability of NG pipelines embedded in sites, similar to Fig. 1. The flowchart of the analytical framework is illustrated schematically in Fig. 2.

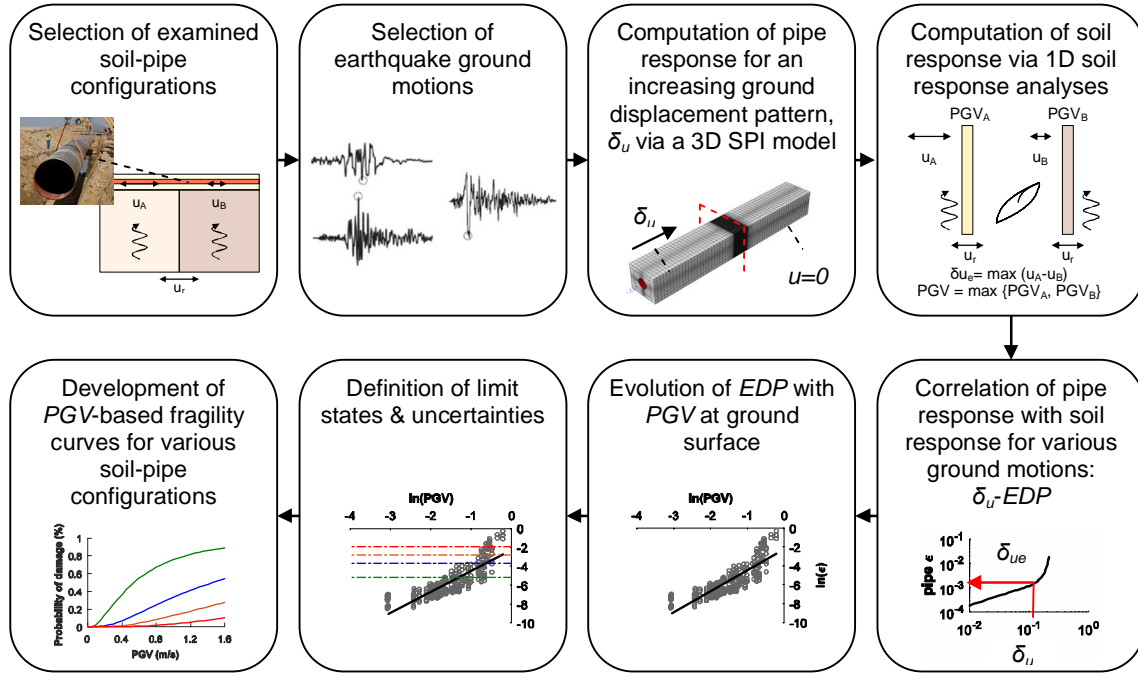


Fig. 2 Flowchart of the analytical framework for the development of fragility curves for buried NG pipelines crossing sites with a geotechnical discontinuity.

The analysis of the seismic response of the selected soil-pipe configurations is carried out in steps, as follows: initially, a 3D trench-pipe numerical model is developed to compute the axial compression response of the buried steel NG pipeline under an increasing level of seismically-induced relative axial ground displacement, δ_u , considering the soil compliance effects. The response of selected soil deposits is then computed by means of separate 1D nonlinear soil response analyses of the adjacent subdeposits. In particular, through the soil response analyses, the horizontal deformations of the subdeposits are computed for the selected ground motions at the burial depth of the examined pipelines. These are subsequently used to define maximum differential ground movement patterns, δ_{ue} , of the soil deposits consisting of the examined subdeposits. The soil response analyses are also used to calculate the peak ground velocity PGV at the ground surface, which is used as seismic intensity measure (IM) to express the fragility curves. The outcomes of the 3D SPI analyses and 1D soil response analyses are finally combined, to correlate the pipe response, in terms of maximum axial compression strain, ϵ , which is selected as engineering demand parameter, EDP , for the pipeline, with the ground response computed for each of the selected pairs of subdeposits and each ground motion. The latter combinations result in relationships of pipe strain ϵ with the PGV at ground surface, which are finally used to define fragility curves for four predefined performance limit states,

considering all the associated uncertainties. The analytical framework is further elaborated in the following sections.

3.2 3D trench-pipe model for SPI analysis

A 3D model of the trench soil, encasing a cylindrical shell model of the pipeline, is initially developed in ABAQUS (2012), aiming at computing the axial response of the pipeline under an increasing level of horizontal relative ground displacement, δ_u , developed near a geotechnical discontinuity (Fig. 3).

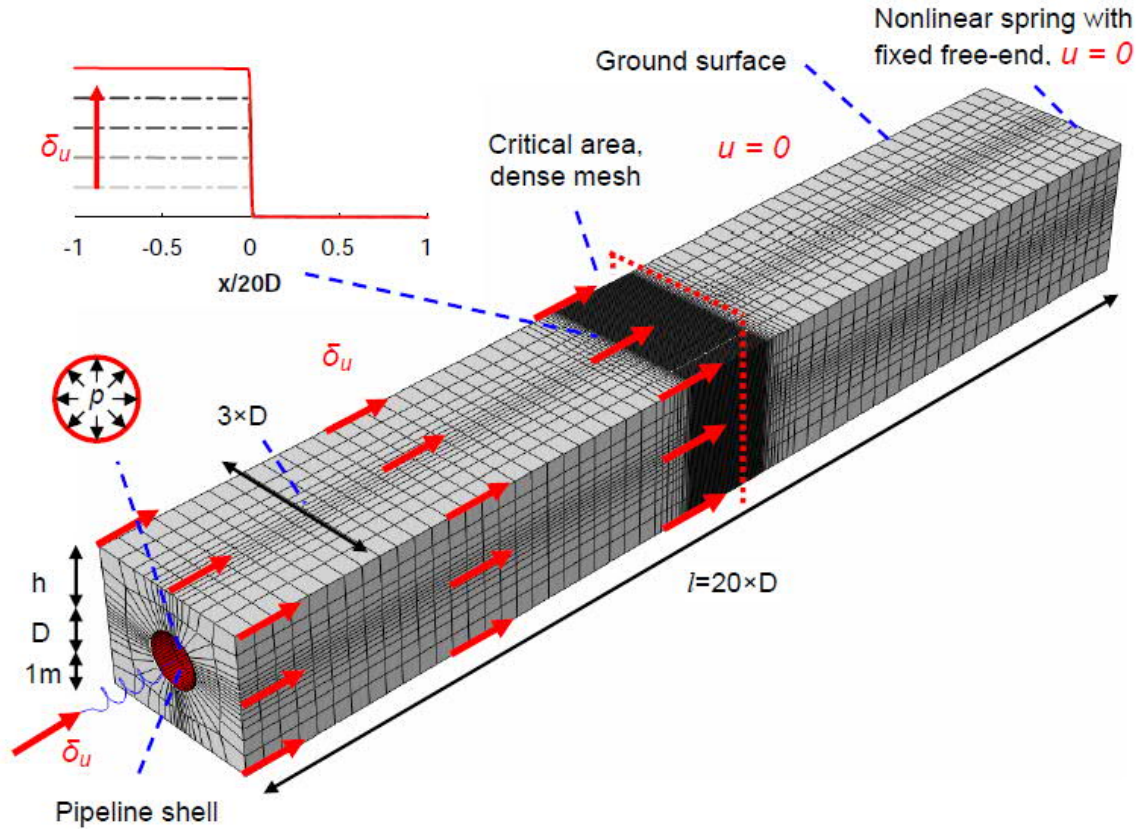


Fig. 3 3D trench-pipe numerical model for the computation of the axial compression response of the pipeline, under an increasing level of seismically-induced relative ground displacement, δ_u .

The use of the near field 3D continuum trench-pipe model allows for a rigorous simulation of localized buckling modes that might potentially be developed in the pipe under axial compression, as well as for the proper simulation of geometric imperfections of the pipeline walls, which are expected to affect significantly the axial compression response of the buried pipeline (Yun and Kyriakides 1990; Tsinidis et al. 2018; Psyrras et al. 2019). Additionally, it allows for a proper simulation of the operational pressure of the pipeline and contact nonlinear phenomena, i.e. sliding and/or potential detachment in the normal direction, between the pipeline wall and the surrounding ground. The latter is of great importance since the shear behaviour of the trench soil-pipe interface effectively controls the level of shear stresses that are transmitted along the perimeter of the pipeline during shaking. The integral of these shear stresses constitutes the axial loading of the pipeline.

3.2.1 Dimensions of the 3D model

The shallow burial depth of the pipeline in addition to absence of significant inertial SSI effects and the assumption of in-plane ground deformation pattern, allow for the simulation of only the surficial soil-trench, which constitutes a surficial block from the semi-infinite 3D ground domain (Psyrras et al. 2019). Along these lines, the distance between the side boundaries of the trench model and the pipe edges is set equal to one pipe diameter, whereas the distance between the pipe invert and the bottom boundary of the trench model is set equal to 1.0 m. Evidently, the distance between the pipe crown and ground surface is defined on the basis of the adopted burial depth, h , of the examined pipeline.

Generally, an ‘adequately long’ 3D continuum model is required to replicate the actual SPI phenomena, accounting for the ‘anchorage’ length of the pipeline on the surrounding trench and its effect on the transmitted shear stresses from the trench on the pipeline through the soil-pipe interface during the axial deformation of the trench. Additionally, there is a requirement of fine discretization of the pipe to adequately resolve the buckling modes of the pipeline, as discussed in the following. The above aspects increase significantly the relevant computational cost of the analysis, even if the seismic loading is considered in a quasi-static manner. To reduce the required length of the 3D model, while accounting for the effect of the infinite pipeline length on the response of the examined pipeline-trench soil configuration, nonlinear springs are introduced at both sides of the pipeline. The force-displacement relation of the nonlinear springs, which are act parallel to the pipeline axis, is given by the following relations:

$$F = \begin{cases} \lambda EA \delta_x & \text{for } \delta_x \leq \frac{\tau_{\max}}{k_s} \\ \lambda EA \frac{\tau_{\max}}{k_s} + \frac{\pi D \tau_{\max}}{m} \left(\sqrt{\left(\lambda \frac{\tau_{\max}}{k_s} \right)^2 + 2m \left(\delta_x - \frac{\tau_{\max}}{k_s} \right) - \left(\lambda \frac{\tau_{\max}}{k_s} \right)} \right) & \text{for } \delta_x > \frac{\tau_{\max}}{k_s} \end{cases} \quad (1)$$

where:

$$\lambda = \sqrt{\frac{\pi D k_s}{EA}} \quad (2)$$

$$m = \frac{\pi D \tau_{\max}}{EA} \quad (3)$$

δ_x is the ground-pipe relative axial movement caused by the relative axial ground deformation δ_u as a result of the dissimilar ground movement of the adjacent subdeposits, τ_{\max} is the maximum shear resistance that develops along the trench backfill-pipe interface, k_s is the shear stiffness of the trench backfill-pipe interface and EA is the axial stiffness of the pipeline cross section. For cohesionless backfills, the maximum shear resistance depends on the adopted friction coefficient μ and varies along the perimeter of the pipe. Average values of τ_{\max} and k_s may be computed on the basis of numerical simulations of simple axial pull-out tests of the examined pipe from the examined trench soil, as discussed later. Following the above simulation approach, the required length of the 3D pipe-soil trench model may be reduced to

20 times the external diameter of the pipeline. The theoretical background behind this simulation approach, which is inspired by a numerical model that was developed by Vazouras et al. (2015), is presented in Tsinidis et al. (2019b). The validity of this proposed simulation is verified in the following, by comparing the stresses and strains computed at the middle critical section of a selected pipeline by the 3D reduced-length model with the nonlinear springs, with relevant predictions of an equivalent quite extended, almost ‘infinitely’ long 3D continuum model of the soil-pipe configuration subjected to the same axial ground deformation pattern. Typical static boundary conditions are applied at the bounding soil surfaces, while the ground surface is set free.

3.2.2 Finite element discretization

The trench soil is simulated by means of hexahedral (brick-type) elements with equivalent soil properties being assign on them (i.e. soil degraded stiffness), the latter being estimated by the separate 1D soil response analyses, as discussed in the ensuing. Inelastic, reduced integration *S4R* shell elements are used to mesh the pipeline. The particular shell elements have both membrane and bending stiffness. The mesh density of the pipeline at the central section of the 3D model, i.e. at the assumed location of the geotechnical discontinuity, where the axial strain of the pipeline is expected to maximize under ground shaking, is selected to be fine enough, so that to resolve the inelastic buckling modes of an equivalent axially compressed unconstrained cylindrical steel shell (Psyrras et al. 2019). To facilitate the selection of mesh, the half-wavelength in the post-elastic range, $\lambda_{c,p}$, is initially computed for the selected pipelines, as per Timoshenko (1961):

$$\lambda_{c,p} \approx \lambda_{c,el} \times \sqrt{E_p/E} \quad (4)$$

where E is the Young’s modulus of the steel grade of the pipeline, E_p is the plastic modulus of the steel grade of the pipeline and $\lambda_{c,el}$ the elastic axial half-wavelength. Considering a Poisson’s ratio $\nu = 0.3$ for the steel grades examined herein, the latter is given as:

$$\lambda_{c,el} \approx 1.72\sqrt{Rt} \quad (5)$$

where R is the radius of the pipeline and t is the wall thickness of the pipeline. Assuming that the plastic modulus E_p is equal to $0.1E$, Eq. 4 yields: $\lambda_{c,p} \approx 0.5\lambda_{c,e}$ (Psyrras et al., 2019). Element lengths, ranging between 1.0 cm and 2.0 cm, depending on the geometric properties of the selected pipelines, were found capable to reproduce the theoretical axial half-wavelength $\lambda_{c,p}$ of the examined pipelines. These mesh seeds are applied over a length of 2.0 m in the middle section of the examined pipelines. The mesh density away from the critical central zone is gradually decreased, with the axial dimension of the shell elements being as high as 0.30 m, in an effort to reduce the computation cost. The mesh discretization of the trench soil in the axial direction of the model matches the exact mesh seed of the pipeline to avoid any initial gaps during the generation of mesh. The mesh seed of the trench in the other two directions is restricted to 0.30 m.

3.2.3 Trench soil-pipe interface

The soil-pipe interface is simulated by means of an advanced hard contact interaction model, available in ABAQUS (2012). The model allows for sliding and/or potential detachment in the normal direction between the interacting pipe and trench-soil elements during the horizontal deformation of the surrounding trench. The shear behaviour of the interface model is controlled by the classical Coulomb friction model, through the introduction of a friction coefficient, μ . The adopted values of friction coefficients, μ , are presented in *Section 4*.

3.2.4 Behaviour of the backfill soil and pipe

The surficial soil-backfill is simulated as an elastic medium, with equivalent properties (i.e. degraded soil stiffness) defined as per *Section 3.3*. The plastic behaviour of the steel pipelines is modelled employing a classical flow plasticity model combined with a von Mises yield criterion. The model is defined by fitting Ramberg-Osgood curves (Equation 6) to bilinear isotropic curves, the latter describing the tensile uniaxial behaviour of the selected steel grades (see *Section 4*)

$$\varepsilon = \frac{\sigma}{E} + a \times \left(\frac{\sigma}{\sigma_y} \right)^n \quad (6)$$

where E is the elastic modulus, σ is the axial stress, ε is the axial strain, σ_y is the yield stress, n is a hardening parameter and a is a ‘yield offset’ which is equal to $\alpha \sigma_y / E$. Parameters a and n are defined for the selected steel grades of the examined pipelines in *Section 4*.

3.2.5 Initial geometric imperfection of the pipeline section

The axial compressive response of thin-walled steel pipelines is known to be highly affected by initial geometric imperfections of the walls (NASA 1968; Yun and Kyriakides 1990; Psyrras et al. 2019). To account for this effect on the structural response of the examined pipelines, both ‘perfect’ pipelines and equivalent pipelines with initial geometric imperfections are examined. For the latter cases, a stress-free, biased axisymmetric imperfection is considered. The imperfection is defined on the basis of a sinusoid modulated by a second sinusoid, as per Equation (7), following Psyrras et al. (2019):

$$\bar{w}(x) = \left[w_0 + w_1 \cos \left(\frac{\pi x}{N \lambda_c} \right) \right] \cos \left(\frac{\pi x}{\lambda_c} \right), \quad -\frac{L_{crit}}{2} \leq x \leq \frac{L_{crit}}{2}, \quad L_{crit} = 2.0m, \quad 2N\lambda_c = L_{crit} \quad (7)$$

The positive values correspond to outward direction from the mid-surface of the pipeline shell wall. The peak amplitude of the imperfection is set as a function of the pipe lining thickness, based on the following formulation: $w = w_0 + w_1 = 0.10t$. The imperfection level is based on relevant specifications from NG pipeline manufactures, e.g., ArcelorMittal specifies a manufacturing tolerance for the walls of API-5L X65 pipelines in the range of + 15% to - 12.5% (ArcelorMittal 2018). The imperfection is applied over the central critical pipeline zone with length equal to $L_{crit} = 2.0$ m, centered at the exact position, where the soil discontinuity is considered. Fig. 4 illustrates a detail of the mesh of the central section of an imperfect pipeline.

The exact same perturbation is introduced on the mesh of the trench soil, surrounding the pipeline, to prevent any initial gaps during the generation of the mesh that might affect the contact phenomena during loading. It is noted that any residual stresses on the pipelines, related to the manufacturing process were disregarded in the present study.

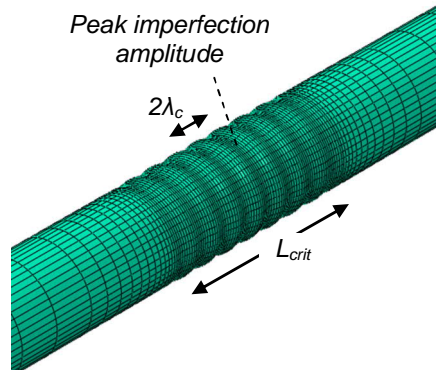


Fig. 4 Detail of the mesh of the central section of a 914.4 mm pipeline with a biased axisymmetric geometrical imperfection of the walls (the radial deformation is exaggerated by a scale factor, i.e. $\times 10$).

3.2.6 Analysis steps

The stress state, associated with the gravity and the internal pressure of the pipeline, is initially established within a general static step. The effect of seismically-induced transient ground deformation is then introduced in quasi-static fashion. In particular, the nodes of the one half of the trench model and the free node of the relevant nonlinear spring are fixed in the axial direction, i.e. the right-hand side of the model in Fig. 3, whereas the nodes of the other half of the trench model and the free node of the relevant nonlinear spring are monotonically forced to move towards constraint part of the model, in a stepwise fashion, thus resulting in a relative axial displacement of the trench model equal to δ_u , the latter increasing throughout the analysis step. The analysis is carried out till the numerical analysis collapses, i.e. after buckling failure of the examined pipeline. This displacement configuration is equivalent to the case, where both halves of the trench model, are moving dissimilarly in the axial direction, causing the same differential axial ground movement δ_u on the examined system. The displacement pattern is kept constant with depth coordinates over the trench soil domain and the free-ends of the nonlinear springs, for the sake of simplicity. This assumption is considered valid since the depth of the trench domain is rather small compared to the predominant wavelength of common seismic waves (Psyras et al. 2019). The above kinematic loading induces shear stresses along the pipe-soil interface, which in addition to the axial loading induced on the both ends of the pipeline through the nonlinear springs, result in an axial compression straining of the pipeline. The latter is traced for the increasing level of relative axial ground displacement, δ_u , via a modified Riks solution algorithm, available in ABAQUS (ABAQUS 2012). Through this analysis, a curve describing the relation between an increasing relative axial ground displacement, δ_u , and the corresponding peak compression axial strain ε of the critical middle section of the pipeline, i.e. near the assumed geotechnical discontinuity, can be established. The peak compression axial strain is evaluated as the envelope of the compression axial strains computed for all the shell elements that are located within the critical section of the pipeline. It

should be highlighted that the analysis focuses on the axial ground displacements and disregards the vertical ones that might be observed near geotechnical discontinuities since the former constitute the dominant loading mechanism for the buried pipeline. Since the response of the pipeline is computed for an increasing level of relative axial ground displacement, δ_{ue} , the outcome of one 3D SPI analysis may be used to examine the axial straining of the pipe under a variety of selected ground axial relative displacements, δ_{ue} , caused by diverse seismic motions. This is of course possible under the assumption and implementation of mean equivalent soil properties for the trench backfill soil, corresponding to the strain-range that is anticipated for the selected ground seismic motions.

3.3 1D soil response analysis of adjacent soil deposits

The response of the selected sites is evaluated through separate 1D soil nonlinear response analyses of the adjacent subdeposits (Fig. 5), carried out by employing the code DEEPSOIL v6.1 (Hashash et al. 2016). The hysteretic nonlinear response of the soil during ground shaking is considered in the analyses by means G - γ - D curves, which are properly selected for the examined deposits, following Darendeli (2001). To avoid the potential amplification of higher frequencies of the ground that may result in unrealistic oscillations of the acceleration time histories in low ground strains, additional viscous damping of 1 % is also introduced in the form of the frequency-dependent Rayleigh type (Hashash and Park 2002). The Rayleigh coefficients are properly tuned for a frequency interval range, characterizing the ‘dominant frequencies’ of each soil column. Through the soil response analyses, time histories of the horizontal deformations of the soil columns are calculated at the burial depths of the pipelines. These time histories are subsequently used to compute maximum differential ground deformation patterns δ_{ue} for the selected pairs of adjusted subdeposits. Additionally, time histories of the horizontal velocity are computed at the ground surface, which are used to evaluate the peak ground velocity PGV at ground surface. The latter is used as seismic intensity measure for the development of the analytical fragility curves.

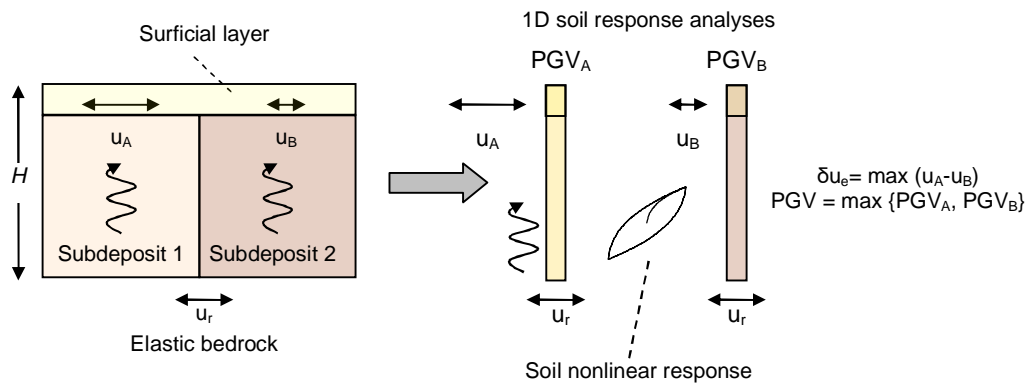


Fig. 5 Schematic view of the analysis framework used to compute the response of the selected soil sites under ground shaking.

3.4 Correlation of 3D SPI and 1D soil response analyses results

The critical relative axial ground deformation patterns, δ_{ue} , which are defined on the basis of the results of the 1D soil response analyses, are correlated with the predicted straining of the

pipeline, using the δ_u -maximum compressive axial strain ε relations computed by the 3D SPI analyses. The identified from the above correlation procedure pipeline strains ε are employed to define ε - PGV relationships, which are finally used to define the numerical fragility curves for predefined limit states in a probabilistic framework, accounting for all the associated uncertainties.

3.5 Performance limit states

The development of analytical fragility curves requires the rigorous definition of performance limit states, which are associated with specific damage levels. In this study, four performance limit states are defined on the basis of peak axial compressive strain ε of the pipeline, following Jahangiri and Shakib (2018). The limit states, summarized in Table 1, refer to different return periods of earthquake, ranging between 25 and 2475 years, and are associated with different levels of damage on the pipeline. They are actually defined on the basis of thorough review of relevant studies, guidelines, codes and regulations, as per Table 1. Despite this fact, the definition of limit states contains a level of uncertainty, which is considered in the definition of fragility curves, as discussed in the ensuing. The first two limit states, i.e. operable limit state (OLS) and pressure integrity limit state (PILS), may be characterized as operational limit states, since no leakages are expected, and the flow of the pipeline is not disrupted. On the contrary, ultimate limit state (ULS) and global collapse limit state (GCLS), constitute ultimate limit states, since pipe wall tearing is expected, resulting in leakages and flow disruption. In terms of damage level, the four limit states may be associated with slight, moderate, extensive and complete damage, respectively. For a more detailed presentation of the relevant definitions of the limit states the reader is referred to Jahangiri and Shakib (2018).

3.6 Development of fragility functions

Fragility functions describe the probability of exceeding different performance limit states, given a level of ground shaking intensity (Elnashai and Di Sarno 2015). Following common approaches, the fragility relations in this study are developed, by employing a lognormal probability distribution function:

$$P(ds \geq ds|S) = \Phi \left[\frac{1}{\beta_{tot}} \times \ln \left(\frac{PGV}{PGV_{mi}} \right) \right] \quad (8)$$

where $P(ds \geq ds|S)$ is the probability of exceeding a particular limit state, ds , for a given seismic intensity level, the latter defined by the peak ground velocity, PGV , at ground surface. Φ is the standard cumulative probability function, PGV_{mi} is the median threshold value of PGV , required to cause the i^{th} damage state, and β_{tot} is the total lognormal standard deviation. Based on the above definitions, the analytical fragility curves may be sufficiently described by defining the following parameters PGV_{mi} and β_{tot} .

Table 1. Limit states adopted Jahangiri and Shakib (2018), t : thickness of the pipeline, D : diameter of the pipeline

Limit state	Maximum limit axial compressive strain	Description	Return period (years)	ε_c defined following:
Operable Limit State (OLS)	$\varepsilon = \min(0.01, 0.4 \times t/D)$	Despite some minor plastic deformations, the pipeline will operate immediately after the event.	25	ALA (2001); JG(G)-206-03 (2004); EN 1998-4 (2006)
Pressure Integrity Limit State (PILS)	$\varepsilon = \min(0.04, 1.76 \times t/D)$	Despite some significant deformations on the pipe, no leakage of containment is taken place.	95	ALA (2001) ; JG(G)-206-03 (2004) ; CEN (2006) ; Mohareb (1995) ; Honegger et al. (2002); Bai and Bai (2014)
Ultimate Limit State (ULS)	$\varepsilon = \min(0.1, 4.4 \times t/D)$	A ‘controllable’ release of the containment of the pipeline is expected.	475	Bai (2001); Honegger et al. (2014); Bai and Bai (2014)
Global Collapse Limit State (GCLS)	$\varepsilon = 0.15$	A structural collapse is reported.	2475	Zhang (2008); Nazami and Das (2010); Ahmed et al. (2011); Bai and Bai (2014)

The fragility curves are established based on the evolution of EDP , i.e. the peak axial strain of the pipeline ε in this study, with increasing earthquake intensity, encountering the associated uncertainties. In particular, PGV_{mi} are defined on the basis of relevant regression analyses of the axial strain of the pipeline ε with increasing PGV at ground surface. The latter is defined in this study as the maximum value of the peak values computed by the 1D soil response analyses of the adjacent subdeposits (see *Section 3.3*). It is worth noticing PGV has been used extensively as seismic IM in fragility relations for buried pipelines (Barenberg 1988; O’Rourke M.J. and Ayala 1993; Eidinger et al. 1995; Eidinger et al. 1998; Jeon and O’Rourke T.D. 1995; ALA 2001; Chen et al. 2002; Pineda and Ordaz 2003; O’Rourke M.J. and Deyoe 2004; Lanzano et al. 2013; Lanzano et al. 2014; Jahangiri and Shakib 2018). The wide use of PGV is attributed to its direct relation with the longitudinal ground strain, which is responsible for the induced damages on buried pipelines caused by transient ground deformations. More importantly, in a recent study of the authors this measure was found to be the optimum one for the structural assessment of buried steel NG pipelines embedded in similar soils sites and subjected to similar seismic hazards. Finally, the metric satisfies the *hazard computability* criterion, since PGV hazard maps are readily available after a major earthquake event.

With reference to the definition of the lognormal standard deviation, β_{tot} , which describes the total variability associated with each fragility curve; three primary sources of uncertainty are considered (NIBS 2004) namely the definition of damage states, β_{ds} , the response and

resistance (capacity) of the element, β_C , and the earthquake input motion (demand), β_D . The total uncertainty is estimated as the root of the sum of the squares of the component dispersions. The uncertainty associated with the definition of damage states, β_{ds} , is set equal to 0.4, following HAZUS suggestions for buildings (NIBS 2004). In a similar manner, the uncertainty due to the capacity, β_C , is assigned equal to 0.25. It is worth noticing that the definition of both β_{ds} and β_C constitutes an open issue, particularly for embedded civil infrastructure (Argyroudis and Pitilakis 2012; Argyroudis et al. 2017). A more rigorous definition of the above parameters requires further detailed investigation, something that is beyond the scope of the present study. The last source of uncertainty, associated with the seismic demand, β_D , is described by the variability in response of the pipeline caused by the variability of ground motion, and it is calculated as the dispersion of the simulated damage indices with respect to the regression fit.

3.7 Limitations

Inevitably, there are some limitations of the analytical framework employed herein. The effects of inertial SPI and of the evolution of stresses and deformations due to temperature changes on the pipeline response, as well as time-dependent phenomena, such as fatigue and steel strength and soil stiffness degradation due to cyclic loading, are neglected. Additionally, the methodology does not account for all the sources that lead to spatial variability of the seismic ground motion along the pipeline axis, such as wave passage effect and loss of coherency. Although the latter parameters may further affect the response of the long buried pipelines, it has been reported that their effect is relatively lower as compared to the effect of soil variability (Psyras et al. 2019). Moreover, complex 2D wave phenomena near the geotechnical discontinuity are not being thoroughly investigated, due to the implementation of 1D soil response analyses. However, 1D nonlinear soil response analyses offer computational efficiency compared to 2D or 3D analyses and may be used as a first approximation for the evaluation of the seismic response of the ground and pipelines at shallow depths (Paolucci and Pitilakis 2007). The computational efficiency of 1D soil response analyses allows for an extended and thorough parametric analysis, such as the one presented in the ensuing. It is also noted that the methodology does not consider the potential effect of the transversal seismic loading on the pipeline response.

4. Numerical parametric study

A comprehensive numerical parametric study was conducted for various soil-pipe configurations, employing the above analytical framework.

4.1 NG pipelines

The external diameter, D , and operational pressure, p , of the examined pipelines were selected on the basis of a preliminary investigation of the variation of these characteristics in case actual transmission NG networks found in several countries of Europe (Table 2). The external diameter, D , wall thickness, t , and examined internal pressures, p , of the selected pipelines are summarized in Table 3. The selected pipelines, which cover a wide range of diameter over

thickness ratios, D/t , that may be found in NG network applications, were designed following the relevant regulations of ALA (2001) for a maximum operational pressure of $p = 9$ MPa. For this maximum pressure level and by setting the external diameter of the pipeline, the wall thickness of the pipeline was calculated. Checks against ovaling due to earth loads were also carried out, as per ALA (2001). It was finally verified that the selected pipeline dimensions are available by the industry. The pipelines are made of API 5L X60, X65 and X70 grades, in an effort to cover a range of steel grades that are commonly used in this infrastructure. The mechanical properties of the selected grades are tabulated in Table 4, while Fig. 6 presents the axial stress-strain curves, which characterize the axial response of the examined pipelines and were defined by fitting Eq. 6 for a yield offset equal to 0.5 %. On this basis, the hardening exponents n are set equal to 15, 19.5 and 21, for grades X60, X65 and X70, respectively. The burial depth, h , of the selected pipelines, i.e. distance between the pipeline crown and ground surface, ranged between 1.0 m and 2.0 m, which constitute common burial depths for this infrastructure.

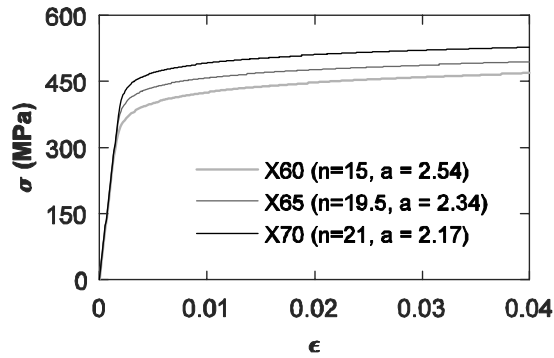


Fig. 6 Uniaxial tensile stress-strain response of API X60, X65 and X70 steel grades adopted herein (n = hardening exponent, a = yield offset $\times E/\sigma_y$).

Table 2 External diameters and range of operational pressure of transmission NG pipeline networks found in several countries of Europe (information provided by the website of each operator).

Country	Operator	Nominal diameter range	Operational pressure range (MPa)
Austria	TAG	914.4 mm to 1066.8 mm (36' - 42')	7 - 8
Belgium	Fluxys Belgium	914.4 mm, 965.2 mm, 1016.0 mm (36', 38', 40')	4 - 7
Germany	Gascade	> 1066.8 mm (42') for the supra-regional networks; otherwise > 508 - 762 mm (20' - 30')	n.p*
Germany	Gasunie	> 1066.8 mm (42') for the supra-regional networks; otherwise > 508 - 762 mm (20' - 30')	n.p
Greece	DESFA	254 mm, 508 mm, 609.6 mm, 762 mm, 914.4 mm (10', 20', 24', 30', 36')	7
Italy	SNAM	508 - 1219.2 mm (20' to 48')	7 - 8
Spain	Enegas	406.4 - 812.8 mm (16' to 32')	n.p
Sweden	Swedegas	406.4 - 660.4 mm (16' to 26')	5 - 8
Switzerland	Transitgas	914.4 - 1066.8 mm (36' to 48')	7 - 8

* n.p.: not provided

Table 3 Dimensions of examined pipes.

External diameter D (°)	External diameter D (mm)	Wall thickness t (mm)	D/t	R/t	Internal pressure, p (MPa)
16	406.4	9.5	42.8	21.4	0, 4, 8
20	508.0	8.7	58.4	29.2	
30	762.0	14.3	53.3	26.5	
36	914.4	12.7	72.0	36.0	
42	1066.8	15.9	67.1	33.55	
48	1219.2	19.1	63.8	31.9	

Table 4 Mechanical properties of steel grades used in this study.

Steel grade	X60	X65	X70
Yield stress, σ_y (MPa)	414	448	483
Ultimate stress, σ_u (MPa)	517	531	565
Ultimate tensile strain, ε_u (%)	14.2	13	11.2
Young's modulus, E (GPa)	210	210	210

4.2 Selected soil sites and backfill of trenches

The depth of the selected soil sites, H , ranged between 30 m, 60 m and 120 m (Fig. 1). Both cohesive and cohesionless soil deposits were examined, with the properties of the examined pairs of subdeposits varying, in order to cover a range of anticipated sites. As stated above, a surficial layer of cohesionless material was considered in all examined cases. This layer, resting upon the examined pairs of subdeposits, had a depth equal to 3.0 m. Additionally, all the examined sites were assumed to rest on an elastic bedrock with mass density, $\rho_b = 2.2 \text{ t/m}^3$ shear wave velocity $V_{s,b} = 1000 \text{ m/s}$.

With reference to the mechanical and physical properties of the subdeposits beneath the surficial layer; Fig. 7 illustrates the gradients of the shear wave propagation velocities and the mass densities, ρ , of the selected soil subdeposits. The variation of the small-strain shear modulus of the cohesionless subdeposits follows the Seed and Idriss (1970) empirical formula:

$$G_{\max} = 220K_{2,\max} (\sigma'_m)^{0.5} \quad (9)$$

where σ'_m is the mean effective confining stress and $K_{2,\max}$ is a constant depending on the relative stiffness D_r of the sub-deposit (Table 5). Using Eq. 9 for the selected soil mass densities and following basic elasto-dynamics, the gradients of small-strain shear wave velocity were defined (Fig. 9a). The gradients of small-strain shear wave velocity of the cohesive soil subdeposits were also considered to increase with depth (Fig. 9b). The selected soil deposits correspond to soil classes B and C according to Eurocode 8 (CEN 2004). The adopted profiles were selected in pairs, in order to define subdeposits 1 and 2 (Fig. 1). In particular, three pairs were examined, i.e. Soil A - Soil B, Soil A - Soil C and Soil B - Soil C. Accounting for the cohesionless and cohesive subdeposits, as well the diverse depths H of the deposits, adopted herein, a total of 18 different cases was finally examined. The nonlinear response of the all selected soil deposits during ground seismic shaking was described by means of adequate G - γ - D curves provided by Darendeli (2001), which were employed in the 1D soil response analyses carried out in DEEPSOIL.

Table 5 Relationships between density, relative density, $K_{2,max}$ parameter and cohesionless soil characterization (after Seed and Idriss 1970).

Density, ρ (t/m ³)	Relative density, D_r (%)	$K_{2,max}$	Characterization
1.4	30	30	Loose
1.65	52.5	48	Medium
2	90	70	Fine

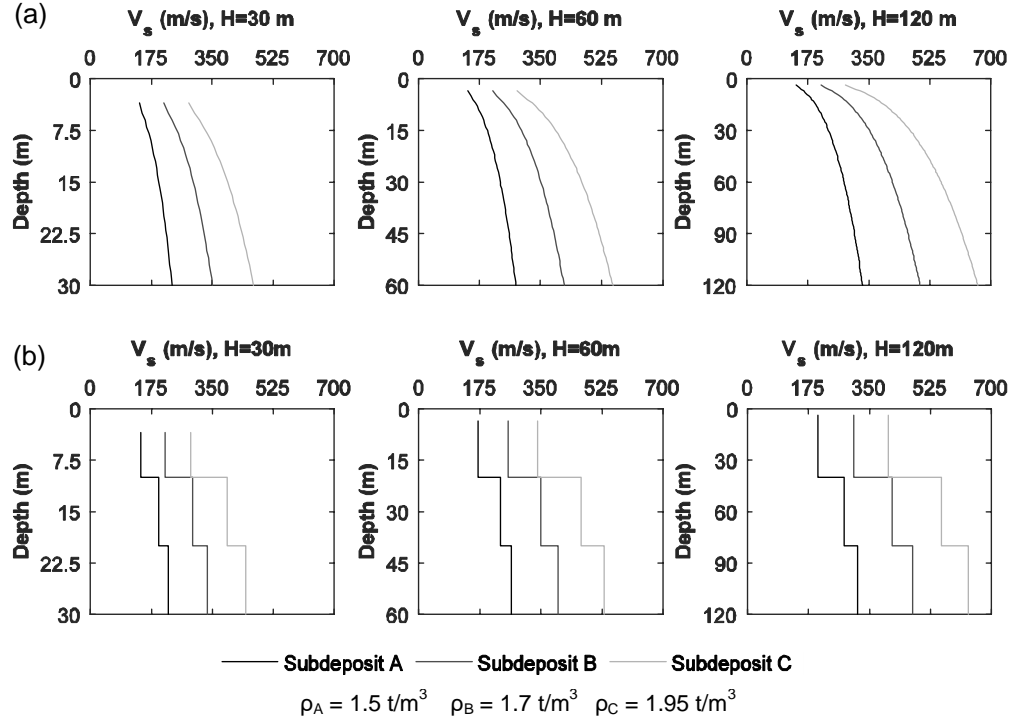


Fig. 7 Shear wave velocity gradients of examined (a) cohesive and (b) cohesionless soil sub-deposits.

Two different sets of mechanical and physical properties were examined for the surficial soil layer. This layer constitutes the trench backfill material for the examined pipelines and therefore is referred as either *trench TA* or *trench TB* in the ensuing, for the sake of simplicity. The selected properties, summarized in Table 6, correspond to well or very well-compacted conditions. For these upper bounds of backfill compaction level, an increased pipeline axial straining is expected under transient ground deformations. It is worth noting that the shear moduli, G , presented in Table 6, correspond to ‘average’ equivalent soil stiffnesses, referring to the ground strain range anticipated for the selected seismic ground motions, and were estimated on the basis of 1D soil response analyses, discussed in *Section 3.3*.

Table 6 Physical and mechanical properties of investigated trenches.

	Density, ρ (t/m ³)	Poisson's ratio, ν	Shear modulus, G (MPa)	Friction angle, ϕ (°)	Friction coefficient, μ
Trench TA	1.65	0.3	37.1	35	0.45
Trench TB	1.9	0.3	63.15	44	0.78

With reference to the selection of the friction coefficient of the trench backfill-pipe interface, μ ; this may vary along the axis of a long-buried pipeline, while it may also change during ground seismic shaking. However, it is bounded between the following limits, $\mu_{min}= 0.3$ and $\mu_{max}= 0.8$. These limits are actually derived from the linear relation between the friction coefficient μ of the soil-pipe interface and friction angle φ of the trench backfill soil, i.e. $\mu = (0.5 - 0.9) \times \tan \varphi$, which was proposed by El Hmadi and O'Rourke MJ (1988) and is commonly adopted in practice (ALA 2001). For typical trench backfills the soil friction angle may range between 29° and $41 - 44^\circ$, yielding to above limits for the friction coefficients. The herein adopted friction coefficients are presented in Table 6.

4.3 Seismic ground motions

An ensemble of 40 real ground motions is used in this study (Table 7), following a relevant selection made by Fotopoulou and Pitilakis (2015), aiming for a diverse, yet unbiased sample of ground motions. The motions were retrieved from the SHARE database (Giardini et al. 2013). The corresponding earthquake moment magnitudes M_w are varying between 5 and 7.62, while the epicentral distances, R , are ranging between 3.4 and 71.4 km. The motions were recorded on rock outcrop or very stiff soil (soil classes A and B according to Eurocode 8, CEN 2004), with shear wave velocity of first 30 m, $V_{s,30}$, ranging between 650 m/s and 1020 m/s. Note that outcrop motions were selected since they were to applied at the bedrock level of the conducted 1D analyses. The input peak ground acceleration PGA varies between 0.065 g and 0.91 g, while the peak ground velocity PGV ranges between 0.031 m/s and 0.785 m/s.

5. Results and discussion

5.1 Verification of the 3D SPI model

The stresses and strains of a representative pipeline predicted under a particular axial ground deformation pattern by implemented the 3D SPI model discussed above, are compared with relevant results of an equivalent 'infinitely' long 3D continuum model of the soil-pipe configuration subjected to the same kinematic loading condition, to verify the efficiency of the selected 3D model. The length of the long 'infinite' model is set equal to 1000 times the external diameter of the pipeline, D , to ensure that its predictions are approaching those of a numerical model with 'infinite' length. In particular, the verification is carried out for a 'perfect' 914.4 mm pipeline, embedded at a burial depth, $h = 1.0$ m in both adopted surficial soil-trenches. The pipeline is pressurized at an internal pressure $p = 8$ MPa. The nonlinear springs that are introduced at the sides of the examined pipeline, as per Fig. 3, are initially defined, as presented in Fig. 8. Fig. 8a illustrates the numerical model used to simulate the axial pull-out of the pipeline. The pull-out analyses are performed examining both adopted surficial soil-trenches, i.e. TA and TB (Table 6). The analyses yield the shear stress-displacement relations provided in Fig. 8b. These relations are used to define the maximum shear resistance τ_{max} and the shear stiffness k_s of the trench-pipe interface, which are subsequently used to define the nonlinear springs, employing Eq. (1). The computed nonlinear

1 springs are presented in Fig 8c. Evidently, a higher friction coefficient for the trench-pipe
2 interface leads to ‘stiffer’ springs.

3 **Table 7.** Selected records used in this study.

Date	Earthquake	Country	Station Name	M _w	R (km)	Preferred FS
25/07/2003	N Miyagi Prefecture	Japan	Oshika	6.1	32.00	Reverse
23/10/2004	Mid Niigata Prefecture	Japan	Tsunan	6.6	36	Reverse
12/06/2005	Anza	USA	Pinyon Flat Observatory	5.2	11.50	Strike-Slip
22/12/2003	San Simeon	USA	Ca: San Luis Obispo; Rec Center	6.4	61.5	Reverse
16/09/1978	Tabas	Iran	Tabas	7.35	57	Oblique
10/06/1987	Kalamata (Aftershock)	Greece	Kyparrisia-Agriculture Bank	5.36	17.00	Oblique
13/05/1995	Kozani	Greece	Kozani	6.61	17	Normal
07/09/1999	Ano Liosia	Greece	Athens 4 (Kipseli District)	6.04	17.00	Normal
15/04/1979	Montenegro	Serbia	Hercegnovi Novi-O.S.D.	6.9	65	Thrust
25/10/1984	Kremidia (Aftershock)	Greece	Pelekanada-Town Hall	5	16	-
17/05/1995	Kozani (Aftershock)	Greece	Chromio-Community Building	5.3	16.00	Normal
13/10/1997	Kalamata	Greece	Koroni-Town Hall (Library)	6.4	48	Thrust
06/05/1976	Friuli	Italy	Tolmezzo-Diga Ambiesta	6.4	21.70	Reverse
15/09/1976	Friuli (Aftershock)	Italy	Tarcento	5.9	8.50	Reverse
23/11/1980	Irpinia	Italy	Bisaccia	6.9	28.30	Normal
14/10/1997	Umbria Marche (Aftershock)	Italy	Norcia	5.6	20.00	Normal
09/09/1998	App. Lucano	Italy	Lauria Galdo	5.6	6.60	Normal
06/04/2009	L Aquila Mainshock	Italy	L Aquila - V. Aterno - Colle Grilli	6.3	4.40	Normal
09/02/1971	San Fernando	USA	Lake Hughes #12	6.61	20.04	Reverse
28/11/1974	Hollister-03	USA	Gilroy Array #1	5.14	11.08	Strike-Slip
06/08/1979	Coyote Lake	USA	Gilroy Array #6	5.74	4.37	Strike-Slip
02/05/1983	Coalinga-01	USA	Slack Canyon	6.36	33.52	Reverse
24/04/1984	Morgan Hill	USA	Gilroy Array #6	6.19	36.34	Strike-Slip
23/12/1985	Nahanni, Canada	Greece	Site 1	6.76	6.8	Reverse
14/11/1986	Taiwan Smart1(45)	Taiwan	Smart1 E02	7.3	71.35	Reverse
07/02/1987	Baja California	USA	Cerro Prieto	5.5	3.69	Strike-Slip
18/10/1989	Loma Prieta	USA	Gilroy Array #6	6.93	35.47	Reverse-Oblique
18/10/1989	Loma Prieta	USA	Ucsc Lick Observatory	6.93	16.34	Reverse-Oblique
25/04/1992	Cape Mendocino	USA	Petrolia	7.01	4.51	Reverse
28/06/1992	Landers	USA	Lucerne	7.28	44.02	Strike-Slip
17/01/1994	Northridge-01	USA	La - Griffith Park Observatory	6.69	25.42	Reverse
17/01/1994	Northridge-01	USA	Pacoima Dam (Downstr)	6.69	20.36	Reverse
16/01/1995	Kobe, Japan	Japan	Nishi-Akashi	6.9	8.7	Strike-Slip
20/09/1999	Chi-Chi, Taiwan	Taiwan	Tcu071	7.62	15.42	Reverse-Oblique
28/06/1991	Sierra Madre	USA	Mt Wilson - Cit Seis Sta	5.61	6.46	Reverse
16/10/1999	Hector Mine	USA	Hector	7.13	26.53	Strike-Slip
20/09/1999	Chi-Chi, Taiwan-03	Taiwan	Tcu129	6.2	18.5	Reverse
17/08/1999	Izmit	Turkey	Gebze-Tubitak Marmara	7.6	42.77	Strike-Slip
17/08/1999	Izmit	Turkey	Izmit-Meteoroloji Istasyonu	7.6	3.40	Strike-Slip
12/11/1999	Duzce 1	Turkey	Ldeo Station No. C1058 Bv	7.1	15.60	Strike-Slip

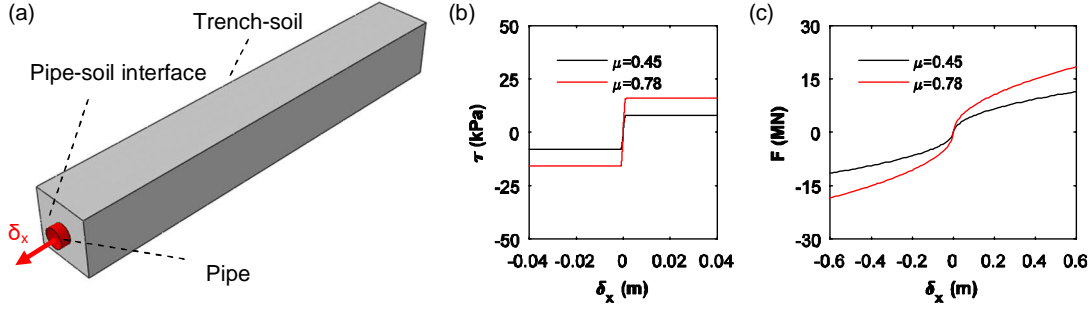


Fig. 8 (a) Numerical simulation of a buried pipeline subjected to axial pull-out, (b) shear stress–displacement relationship at the pipe-soil interface computed for the $D = 914.4$ mm pipeline, embedded in trench soil TA ($\mu = 0.45$) and TB ($\mu = 0.78$) in burial depth $h = 1.0$ m, (c) force-displacement relation of the nonlinear springs computed for the $D = 914.4$ mm pipeline, embedded in trench soil TA ($\mu = 0.45$) and TB ($\mu = 0.78$), $h = 1.0$ m.

Fig. 9 compares contour diagrams of the Mises stresses and axial strains computed at the critical central section of the pipeline by the two numerical models for a relative axial ground deformation $\delta_u = 20$ cm. The reduced-length 3D model SPI model with the nonlinear spring at the sides of the pipeline provides quite similar –if not identical– results with the extended-length 3D SPI model, both in terms of stresses and strains, irrespectively of the assumed trench properties. Naturally, a higher axial response of the pipeline is reported for surficial soil-trench TB, where a rougher soil-pipe interface is considered. Evidently the computational cost of the reduced length model is significantly lower than that of the extended model. It is worth noticing that similarly good comparisons between the predictions of the reduced length 3D model with the nonlinear springs at both ends and the ‘infinitely’ long 3D model were observed, even when a geometric imperfection was considered on the central critical sections of the pipeline.

Fig. 10 elaborates on the effect of the selected width and depth of the trench soil model, surrounding the pipeline, by comparing contour diagrams of the axial straining computed on an examined pipeline, for different widths and depths of the trench continuum model. The results refer to a 762 mm ‘perfect’ pipeline embedded in surficial soil-trench TA at a burial depth $h = 1.0$ m. The pipeline is pressurized to an internal pressure $p = 8$ MPa and is subjected to a relative axial ground deformation $\delta_u = 20$ cm. The length of the models remains constant in all the examined cases, while nonlinear springs are properly defined as per Fig. 8 for each examined ‘trench dimensions’. For the displacement loading patterns examined herein, the differences on the predictions of the pipeline axial strains are very small, if not negligible.

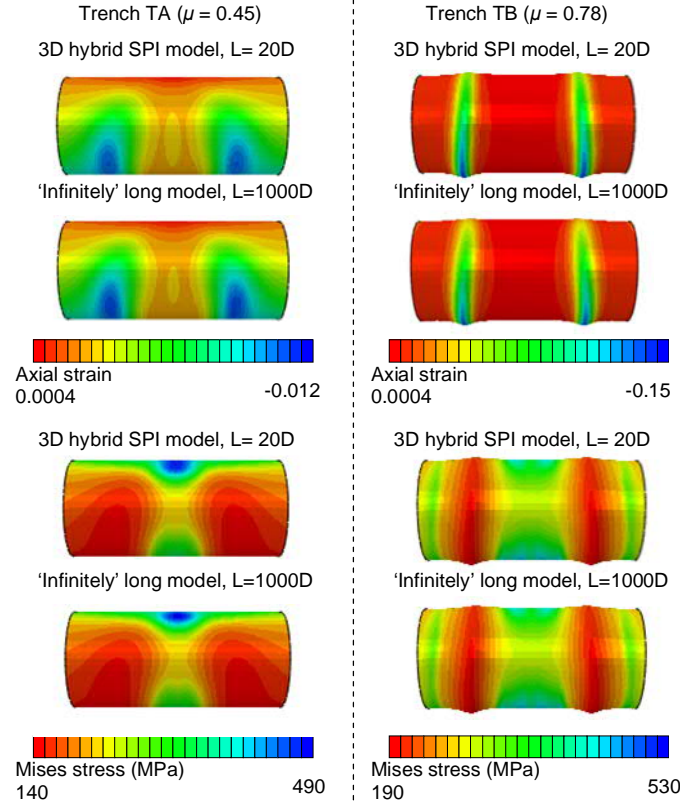


Fig. 9 Comparisons of contour diagrams of the Mises stresses and axial strain distributions computed at the critical central section of a 914.4 mm pipeline, embedded in backfill TA or TB, by the 3D SPI model with the nonlinear springs at both end sides and an 'infinitely' long equivalent 3D SPI model.

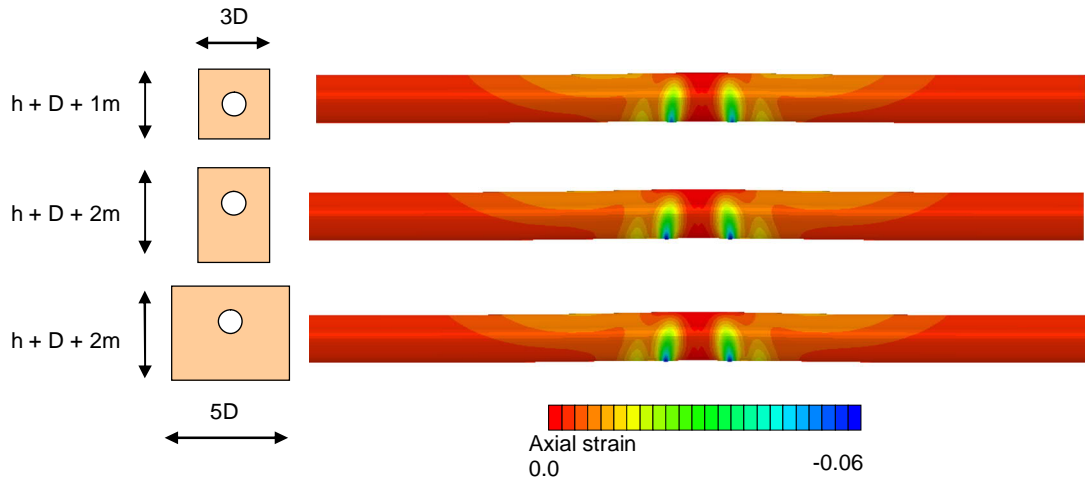


Fig. 10 Contour diagrams of axial strains distributions computed on 762 mm 'perfect' pipeline embedded in trench TA, pressurized to an internal pressure $p = 8$ MPa and subjected to a relative axial ground deformation $\delta_u = 20$ cm, using 3D trench-soil models of diverse widths and depths.

5.2 Pipeline response under an increasing relative axial deformation of the surrounding ground

Fig. 11 illustrates some representative results from 3D SPI analyses of a 1219.2 mm pipeline, embedded in surficial soil-trench TB at a burial depth, $h = 1.0$ m, elaborating on the effect of salient parameters on the axial response of embedded steel pressurized pipelines under an increasing relative axial ground deformation. In particular, contour diagrams of the axial stresses, developed at the critical zone of the pipeline, are plotted for two distinct steps of the analysis, i.e. before major concentration of stresses and buckling failure at the zone and at the end of the analysis, after buckling failure occurrence (end of analysis). The diagrams are plotted on the deformed shapes of the pipelines, so that to highlight the form of buckling failures that occur for higher levels of imposed relative axial ground deformations. Additionally, the figure portrays the evolution of maximum compressive strain of the critical pipeline zone with increasing relative axial ground deformation δ_u . The results are provided for various levels of internal pressure for the pipeline (i.e. $p = 0, 4$ MPa and 8 MPa), considering both a ‘perfect’ pipeline (i.e. $w/t=0$) and an equivalent imperfect pipeline (i.e. $w/t=0.1$). Evidently, both the pressurization level of the pipeline and the initial geometric imperfections of the pipeline wall affect the axial response of the examined pipelines.

In particular, with increasing relative axial ground deformation δ_u , the pipeline tends to bend upwards, i.e. towards the free ground surface. This response results in an early concentration of compressive axial stresses at the invert part of the pipeline, i.e. ditch axis of the pipeline. The existence of geometric imperfections is found to affect the distribution of the axial stresses on the pipeline. Actually, these stresses tend to distribute more uniformly across the invert of the perfect pipeline. On the contrary concentrations of stresses are observed at the imperfection ‘bulges’ of the imperfect pipeline.

The pressurization level tends to affect the buckling patterns of the examined pipelines, which take place under large relative axial ground deformations, i.e. $\delta_u \approx 12 - 20$ cm for the examined cases. Inward deformations of the pipe walls (i.e. deformations towards the pipe cavity) are observed for the non-pressurized (i.e. $p = 0$ MPa) or the low pressurized (i.e. $p = 4$ MPa) pipelines, while a combination of inward and outward deformations (i.e. deformations towards the trench soil) are observed on the highly pressurized pipelines (i.e. $p = 8$ MPa).

The effects of the wall imperfections and internal pressure are also evident on the evolution of maximum compressive axial strain of the critical zone of the pipeline with the increasing relative axial ground deformation δ_u . Higher strains are reported on the pressurized pipelines even at low δ_u , compared to those predicted on the non-pressurized pipelines. This observation is related to the combined effects of the operational internal pressure and axial compression of the pipeline caused by the seismic ground movement, on axial response of a steel pipeline (Paquette and Kyriakides 2006; Kyriakides and Corona 2007; Tsinidis et al. 2018). Additionally, the pipeline with the wall imperfection tends to concentrate higher strains throughout the analysis compared to the equivalent ‘perfect’ pipeline, with the differences between the two cases being as high as 18 %.

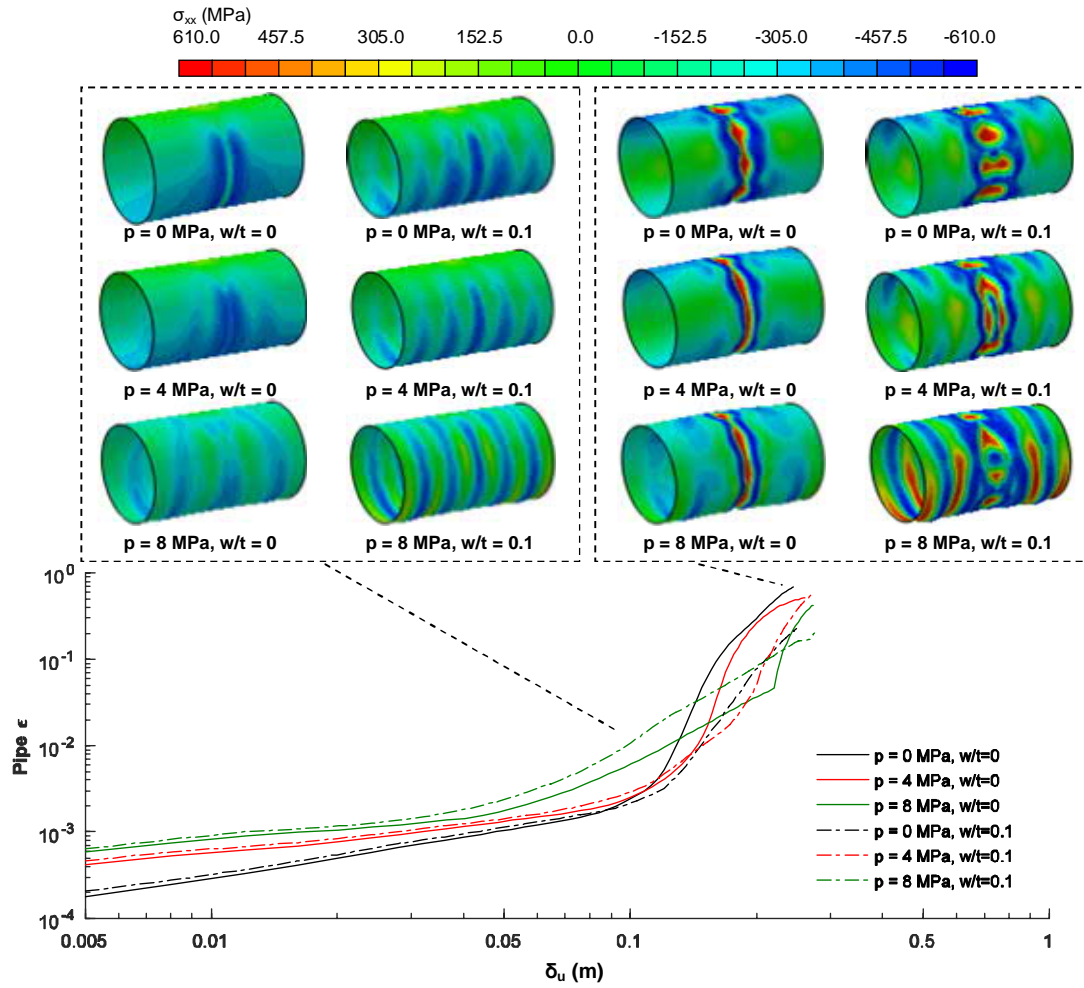


Fig. 11 Effects of internal pressure and geometric imperfection of the pipe walls on the axial stresses and the evolution of the maximum compressive strain, computed at the critical pipeline section for an increasing relative axial ground deformation δ_u (results for a $D = 1219.2$ mm pipeline, embedded in trench TB at a burial depth, $h = 1.0$ m).

Fig. 12 presents comparisons of relations of maximum pipeline compressive strain, ϵ , with increasing relative axial ground deformation δ_u , as computed by 3D SPI analyses. The relations are plotted for 406.4 mm and 1219.2 mm ‘perfect’ or ‘imperfect’ pipelines embedded at various depths, h , in surficial backfill soils TA and TB and pressurized to various levels, i.e. $p = 0, 4, 8$ MPa. The comparisons highlight the critical effects of pipeline dimensions, backfill properties and compaction level and backfill-pipe interface friction characteristics on the axial response of the steel pipelines, induced by seismically-induced relative axial ground deformations. Evidently, higher axial compression strains, ϵ , are reported for the pipelines embedded in backfill TB. The higher shear stresses that are developed along the ‘rougher’ backfill-pipe interface (the friction coefficient μ is equal to 0.78 in this case), result in an increased axial straining of the pipelines embedded in these surficial soil conditions, compared to the equivalent pipelines embedded in trench TA. Additionally, the higher confinement that is being offered by the surrounding ground on the pipeline, as a result of its higher compaction

level and stiffness, partially reduces the upward bending of the pipeline during the kinematic loading of the system (i.e. bending towards the ground surface, see Fig. 9), which in turn leads to an increased localization of axial straining at the critical zone of the pipeline, near the geotechnical discontinuity. Additionally, the concentration of axial compression strains, which subsequently leads to buckling of the pipelines, occurs in higher levels of relative axial ground deformation, δ_u , in the case of 1219.2 mm pipelines with thicker walls. It is worth noticing the wide range of pipeline strain ϵ that might be computed for a given level of relative axial ground deformation, δ_u , under various assumptions regarding the initial geometric imperfections of the pipeline walls, the backfill properties, the backfill-pipe interface characteristics and the internal pressure of the pipeline. Indeed for a given relative axial ground deformation $\delta_{ue,n}$ in Fig. 12 (associated with a ground motion and computed by the 1D soil response analyses as per Section 3.3), a wide range of compressive strains ϵ may be computed on the pipeline, when considering all the above parameters. Hence, the consideration of these parameters is of great importance in the structural vulnerability assessment of this infrastructure.

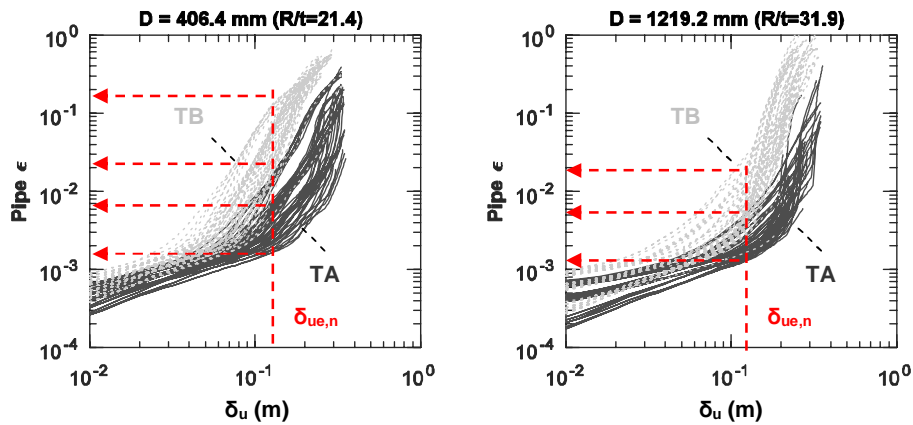


Fig. 12 Evolution of the maximum compressive strain, ϵ , computed at the critical middle section of ‘perfect’ or ‘imperfect’ pipelines, embedded at various depths, h , in surficial backfill soils TA and TB and pressurized to various levels, i.e. $p = 0, 4, 8$ MPa, for an increasing relative axial ground deformation δ_u .

5.3 Fragility functions

Prior to the development of the fragility functions, the limit states defined in Section 3.5, are quantified for the selected pipelines, as per Table 1. Table 8, summarizes the limit axial compression strains for the four limit states for all examined pipelines. As seen, the maximum strain for OLS may range between 0.56 % and 0.94% for the examined pipelines. The range of strains for PILS varies between 2.4 % and 4 %, while for ULS the limit strain ranges between 6.1 % and 10 %.

Table 8 Quantification of the maximum compression axial strains defined for each limit state and examined pipeline.

Diameter, D (mm)	406.4	508	762	914.4	1066.8	1219.2
Wall thickness, t (mm)	9.5	8.7	14.3	12.7	15.9	19.1
R/t	21.4	29.2	26.6	36.0	33.5	31.9
Maximum strain for limit state OLS, ϵ_{OLS}	0.0094	0.0069	0.0075	0.0056	0.0060	0.0063
Maximum strain for limit state PILS, ϵ_{PILS}	0.0400	0.0301	0.0330	0.0244	0.0262	0.0276
Maximum strain for limit state ULS, ϵ_{ULS}	0.1000	0.0754	0.0826	0.0611	0.0656	0.0689
Maximum strain for limit state GCLS, ϵ_{GCLS}	0.1500	0.1500	0.1500	0.1500	0.1500	0.1500

Having quantified the maximum strain for each limit state and examined pipeline, regression analyses of the natural logarithm of the computed maximum axial strain ϵ of the examined pipeline relative to the natural logarithm of the peak ground velocity PGV at ground surface are carried out, as per Fig. 13. The regressions are actually conducted for each soil-pipe configuration, by combining the numerical predictions of the above analytical framework, referring to various levels of internal pressure for pipelines (i.e. $p = 0, 4$ and 8 MPa) and various assumptions regarding the initial geometric imperfection of the pipeline walls (i.e. combining the results referring to $w/t = 0$ or $w/t = 0.1$). The selection is made on the ground that existence of geometric imperfections on pipeline walls is not a-priori known. Additionally, the use of results, referring to a range of internal pressures, allows for a general application of the provided fragility curves in networks with similar ranges of operational pressure. The results of the regression analyses are used to define the parameters that are required to construct the fragility functions, i.e. PGV_{mi} and β_{tot} .

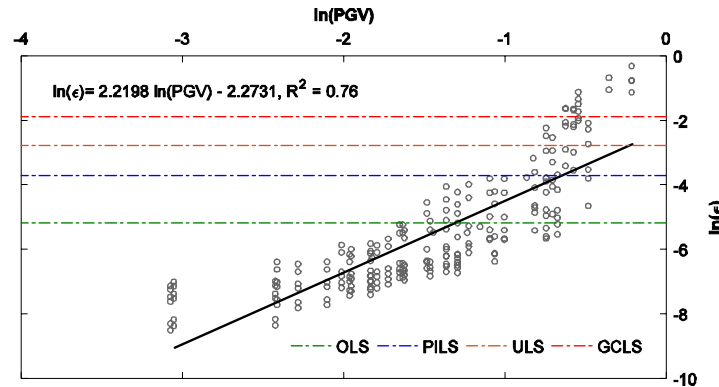


Fig. 13 Example of evolution of $\ln(\epsilon)$, with earthquake intensity measure $\ln(PGV)$ and regression analysis used to define PGV_{mi} and β_{tot} (numerical results for of a 762 mm pipeline embedded in Trench TA at a burial depth, $h = 1.0$ m in soil deposit with depth $H = 30$ m)

Based on the above procedure, an extended set of more than 1200 fragility functions was constructed, referring to diverse examined soil-pipe configurations. The relevant PGV_{mi} and β_{tot} for all the examined curves are summarized in a set of tables, summarized in Appendix A. In the following, some representative fragility curves are comparatively presented, aiming at

1 discussing the effects of salient parameters on the computed fragility of the examined NG
2 pipelines.

3 Fig. 14 compares analytical fragility relations, referring to X65 914.4 mm pipelines embedded
4 in surficial soil-trench TA, highlighting the effects of the depth, H , of the soil deposit, the
5 subdeposits characteristics and pipeline burial depth h , on the seismic fragility of NG pipelines.
6 Generally, the seismic fragility of the examined pipelines is found to be low. Actually, the ULS
7 and GCLS limit states are not reached for the examined pipelines embedded in soil deposits
8 with depths, H , equal to 30 m and 60 m, while the seismic fragility of examined pipelines is
9 found to increase with increasing burial depth, H , of the soil deposit. This observation is
10 attributed to the higher differential ground response of the adjacent subdeposits, expected for
11 deposits with higher depths, i.e. for $H = 120$, compared to the one of deposits with depths, H ,
12 equal 30 m or 60 m, when subjected to the same excitation at the bedrock. The higher
13 differential ground response of the adjacent subdeposits induces a higher axial straining on the
14 pipeline, thus increasing the potential of damage under a given seismic intensity.

15 The seismic fragility of the examined pipelines embedded in cohesionless soils is found to be
16 slightly lower compared to the one predicted for the cases where the pipelines are embedded in
17 cohesive soils (see subplots on the left-hand side of Fig. 14). The differences are again
18 attributed to the distinct ground response characteristics of the examined soil subdeposits,
19 which induce distinct axial straining on the embedded pipelines.

20 The higher contrast on the soil properties of the adjacent soil subdeposits, leads naturally to a
21 more dissimilar response of the subdeposits, which induces a higher straining on the pipeline,
22 thus resulting in a higher potential for damage, under a given intensity. This hypothesis is
23 verified by comparing the fragility curves developed for the pairs of subdeposits A-B and A-C.
24 Indeed, a higher fragility is reported in case of pipelines embedded in soil with subdeposits A-
25 C, where the differences on the soil properties of the subdeposits (i.e. shear wave velocity and
26 mass density) are higher compared to the case of the soil that consists of subdeposits A-B.
27 Comparing the fragility of pipelines embedded in soils with subdeposits A-B and B-C, a much
28 higher fragility is reported in the former soil site, even though the level of contrast of the
29 properties of the adjacent subdeposits is the same for both cases. This is actually expected,
30 given the lower ground seismic response of 'stiffer' soil deposits, i.e. the soil with subdeposits
31 B-C in this case, compared to soft soil deposits (i.e. soil with subdeposits A-B), under a given
32 seismic intensity.

33 A higher fragility is systematically reported for pipelines embedded at a burial depth, $h = 1.0$
34 m, compared to the cases, where the equivalent pipelines are embedded deeper, i.e. $h = 2.0$ m.
35 This should be attributed to the higher horizontal ground movement of the soil deposits
36 towards the ground surface, during ground shaking, which causes higher relative ground
37 deformations on the shallow-buried pipelines, hence increasing their axial response and
38 damage potential.

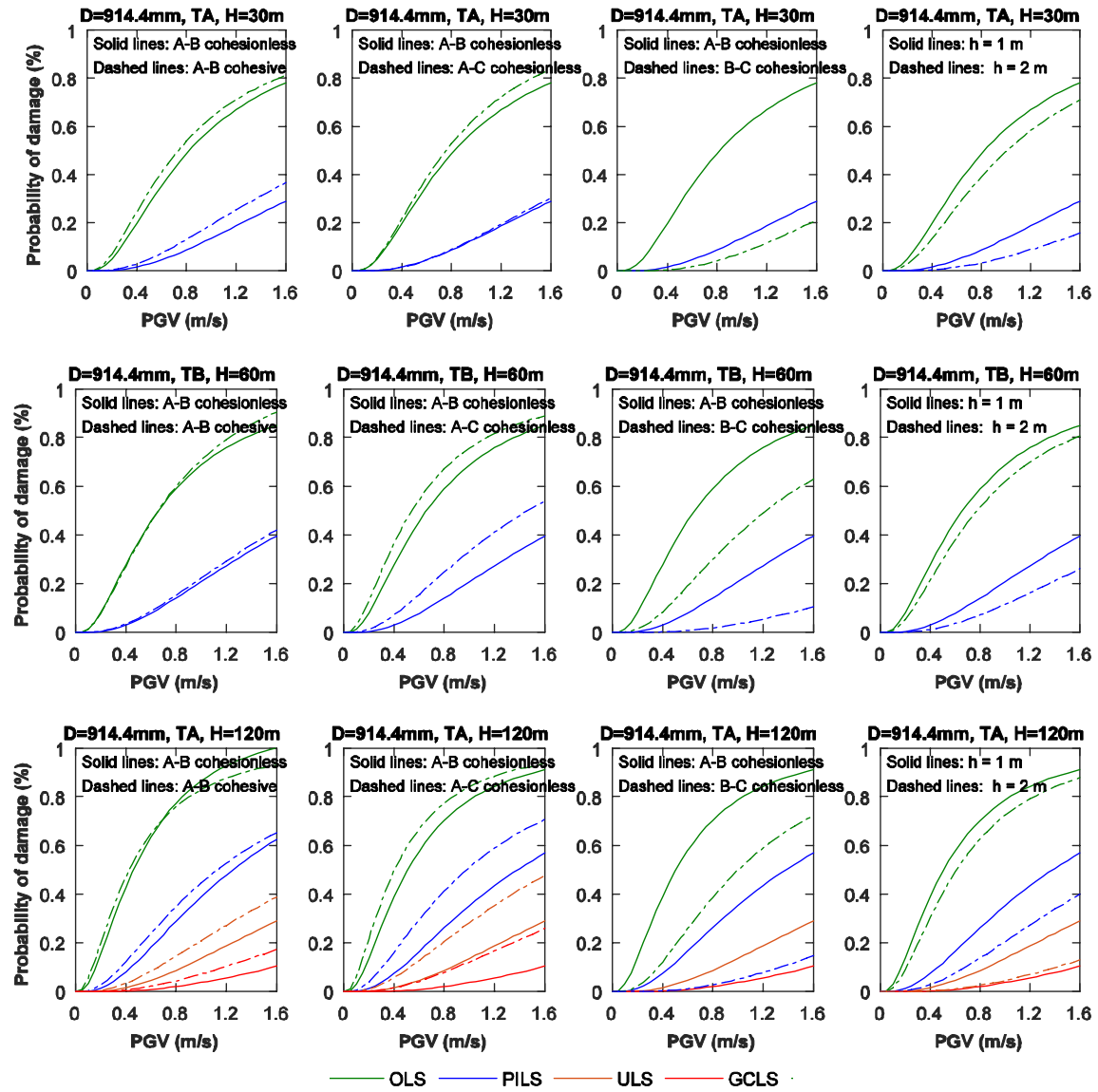


Fig. 14 Fragility functions of X65 914.4 mm pipelines embedded in surficial soil-trench TA. Effects of soil deposit depth, H , subdeposits characteristics and burial depth, h , of the pipelines on the seismic fragility.

It is worth noticing that the general low fragility of the buried pipelines in surficial soil-trench TA comes in line with the reported good performance of buried NG pipelines and their reduced fragility reported during past earthquakes. It is recalled that the first two limit states, adopted in this study, constitute operational limit states that do not lead to wall tearing and leakages and basically do not affect the flow of containment - at least not significantly. This makes the observation of relevant actual damages rather difficult after an earthquake event.

Fig. 15 compares similar fragility relations, referring to the same pipelines, i.e. X65 914.4 mm pipelines, embedded in surficial soil-trench TB. Evidently, a much higher fragility is reported in this case, compared to the previous results. All limit states are reached, even for the cases where the pipelines are embedded in the shallow soil deposits, i.e. for $H = 30$ m and 60 m. This observation is in line with the higher axial compressive straining of the pipeline that is

anticipated in cases of a dense backfill trench with a ‘rougher’ backfill-pipe interface (i.e. surficial soil-trench TB). In line with the previous results, the fragility of the examined pipelines is increased with increasing depth of the soil deposits, H , decreasing burial depth of the pipelines, h , and increasing contrast of the properties of the adjacent soil subdeposits. A slightly higher fragility is reported for the pipelines embedded in the soil deposits with cohesive subdeposits. It is worth noting that higher total lognormal standard deviations β_{tot} were estimated for the fragility relations referring to pipelines embedded in surficial soil-trench TB, associated with the generally amplified axial response of pipelines for these conditions.

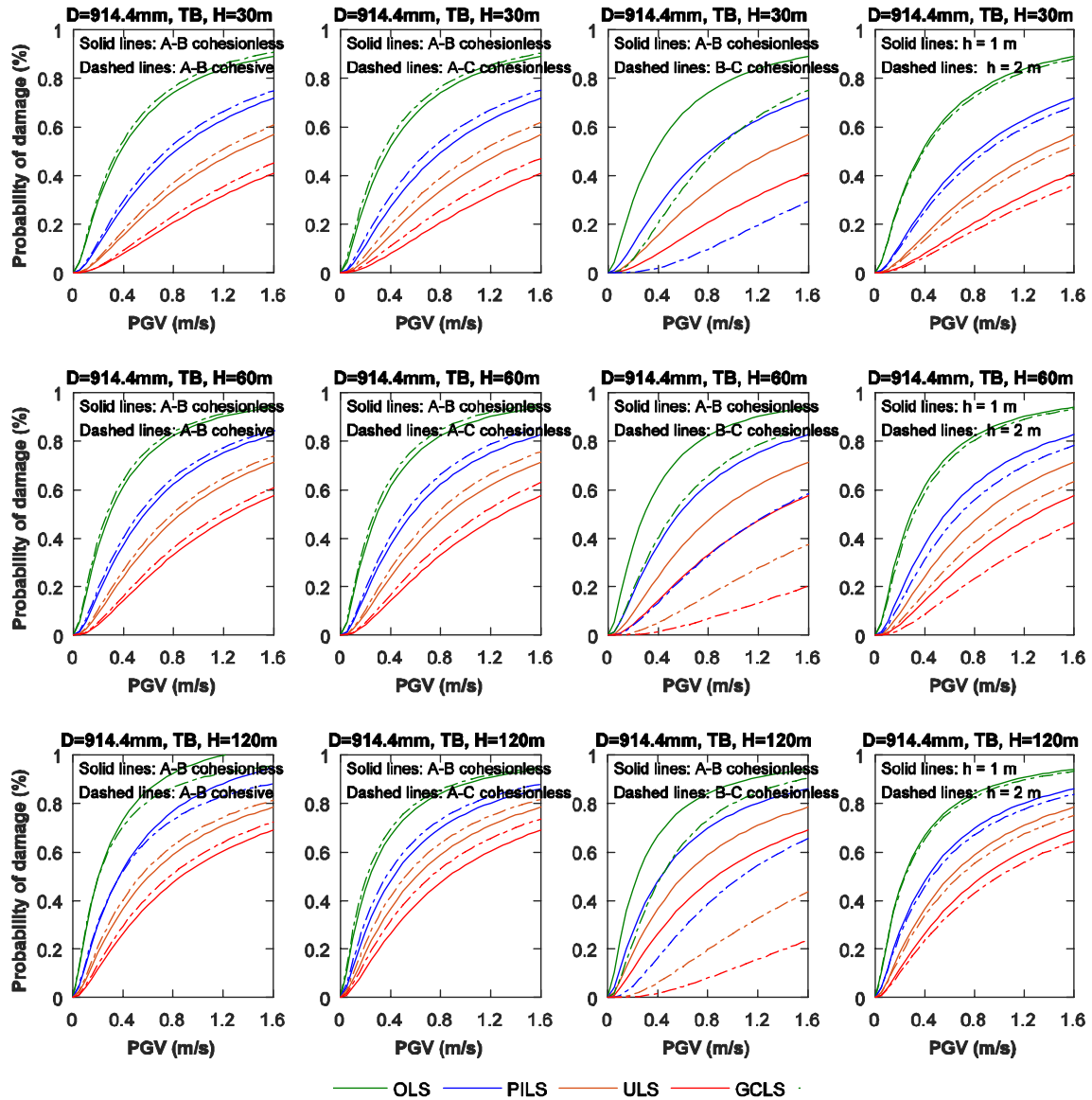


Fig. 15 Fragility functions of 914.4 mm X65 pipelines embedded in surficial soil-trench TB. Effects of soil deposit depth, H , subdeposits characteristics and burial depth, h , of the pipelines on the seismic fragility.

The effect of the steel grade of the pipeline on its fragility is highlighted in Fig. 16, where fragility curves referring to 762 mm pipelines made of different steel grades, i.e. X60 and X70, are compared. The comparisons refer to pipelines embedded in surficial soil-trench TB in cohesive or cohesionless soil deposits A-B of depth $H = 60$ m. As expected, the fragility of X60 pipelines is found higher, compared to the equivalents made of X70 steel grade.

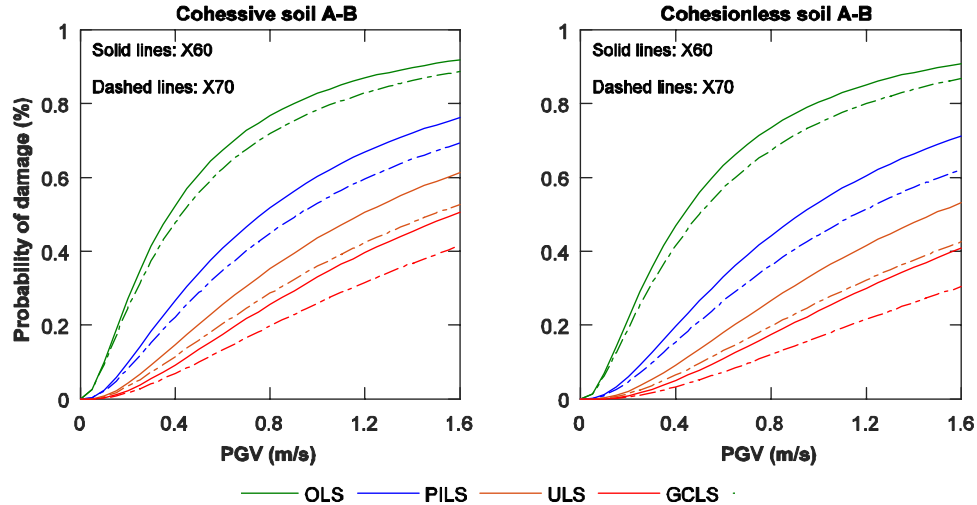


Fig. 16. Effect of steel grade of pipelines on their seismic fragility. Fragility functions for 762 mm pipelines embedded in surficial soil-trench TB in cohesive or cohesionless soil deposits A-B of depth $H = 60$ m.

Fig. 17 compares fragility relations, referring to pipelines with diverse dimensions, embedded in similar trench soil conditions and burial depth, h , (i.e. soil deposit A-B of depth $H = 60$ m and pipeline burial depth $h = 1.0$ m), in an effort to highlight the effect of the radius over thickness ratio (R/t) of the pipelines on their seismic fragility. The comparisons do not provide a clear trend between the radius over thickness ratio (R/t) of the pipeline and its seismic fragility. Indeed, the highest fragility is reported for the 914.4 mm pipelines with $R/t = 36$, followed by the 406.4 mm pipelines with $R/t = 21.4$. The lowest fragility is reported for the 1219.2 mm pipelines with $R/t = 31.9$.

6. Conclusions

A detailed analytical framework was developed to evaluate the fragility of NG pipelines crossing sites with a vertical geotechnical discontinuity, when subjected to axial compression caused by transient seismic ground deformation. The methodological framework consists of a 3D SPI model, aiming at evaluating the pipe-trench interaction effects on the pipeline axial response in quasi-static manner and 1D soil response analyses, used to determine critical ground deformation patterns at the geotechnical discontinuity under ground shaking. The efficiency of the 3D SPI model in replicating the actual soil-pipe interaction phenomena, associated with the extended length of this infrastructure was thoroughly verified. A comprehensive parametric analysis was performed, using the proposed analytical framework, for an extended number of soil-pipe configurations and an ensemble of 40 recorded earthquake

ground motions, which led to the definition of an extended set of fragility curves. The latter were developed in terms of PGV at the ground surface, for four performance limit states, considering the associated uncertainties. The main conclusions of the study are summarized in the following:

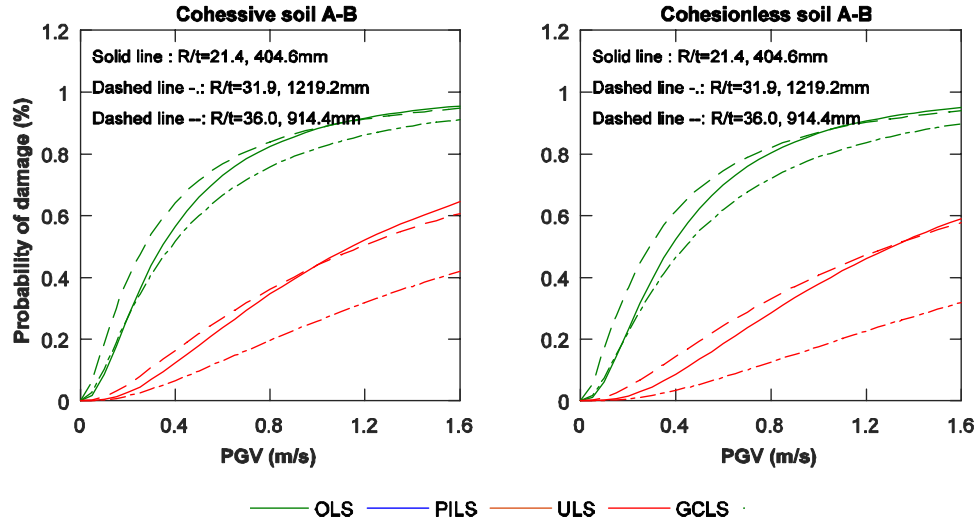


Fig. 17. Effect of radius over thickness (R/t) ratio of diverse pipelines, embedded in trench TB in cohesive or cohesionless soil deposits A-B of depth $H = 60$ m, on their seismic fragility.

- The seismic fragility of buried steel NG pipelines against seismically-induced axial compression near geotechnical discontinuities was found to be rather low, when the examined pipelines were embedded in a medium-compacted surficial layer with a medium friction coefficient μ being considered for the trench soil-pipe interface (i.e. surficial soil-trench TA in this study). Actually, for these cases, the ULS and GCLS limit states, which are associated with major failures or collapse were not reached in the majority of the examined soil-pipe configurations. This observation is in line with the reduced vulnerability of this infrastructure against transient ground deformations, reported during past earthquakes.
- On the contrary, a higher fragility was reported for the pipelines embedded in a ‘stiffer’ very well-compacted surficial soil-trench, with a high friction coefficient μ being considered for the trench soil-pipe interface (i.e. surficial soil-trench TB). This is mainly attributed to the higher axial straining of the pipeline, which is caused by the higher stresses developed along the trench-pipe interface during the surrounding ground deformation. Additionally, the higher compaction level and stiffness of the surrounding ground lead to a higher confinement of the pipeline, which reduces the bending of the pipeline towards the ground surface, during the kinematic loading of the system, thus increasing the local straining of the pipeline, finally contributing to an increased damage potential. In the light of the above observations, it is very important to avoid over-compacting of the trench soil of buried NG pipelines, or even try to reduce the soil-pipe interface friction, particularly in seismically-prone regions of varying soil conditions, in

order to reduce the fragility of this infrastructure under seismically-induced transient ground deformations.

- Regardless of the trench backfill properties and backfill-pipe interface characteristics the seismic fragility of the examined NG pipelines was increased with increasing depth, H , of the soil deposit. This was attributed to the higher differential ground response of deeper adjacent subdeposits, e.g. for $H = 120$ m, under a given excitation at bedrock. The higher differential ground response of the adjacent subdeposits induced a higher axial straining on the pipeline, thus increasing the potential of damage.
- The seismic fragility of pipelines was found to be slightly lower for the cohesionless subdeposits, studied herein, compared to the one predicted for equivalent pipelines in cohesive subdeposits.
- The higher contrast on the soil properties of the adjacent soil subdeposits, led to a more dissimilar seismic response of the subdeposits under a given excitation at bedrock, which subsequently led to a higher axial straining for the embedded pipeline and hence to a higher damage potential.
- A higher fragility was systematically reported for pipelines embedded at a burial depth, $h = 1.0$ m, compared to the cases, where the equivalent pipeline was embedded at a higher depth, i.e. $h = 2.0$ m. Naturally, pipelines made of X60 steel grade were found to be more vulnerable to the particular seismic hazard, compared to those made of higher steel grades, e.g. X65 and X70, while it was not possible to define a clear trend between the radius over thickness (R/t) of the pipeline and its seismic fragility.

Inevitably, there are some limitations of the analytical framework used herein. The effects of inertial SPI and of the evolution of stresses and deformations due to temperature changes on the pipeline response, as well as time-dependent phenomena, such as fatigue and steel strength and stiffness degradation due to cyclic loading, are not considered in the present analysis framework. Moreover, complex 2D wave phenomena near the geotechnical discontinuity are not being thoroughly investigated. However, the study covers a wide range of salient parameters that may affect the response and vulnerability of buried steel NG pipelines, crossing similar sites. In this context, the use of the provided analytical fragility curves may contribute towards a more reliable quantitative risk assessment of buried steel NG pipelines, subjected to seismically-induced transient ground deformations, particularly if combined with the practical recommendations reported above.

Acknowledgements

This work was supported by the Horizon 2020 Programme of the European Commission under the MSCA-RISE-2015-691213-EXCHANGE-Risk grant (Experimental and Computational Hybrid Assessment of NG Pipelines Exposed to Seismic Hazard, www.exchange-risk.eu). This support is gratefully acknowledged.

References

- ABAQUS (2012) ABAQUS: theory and analysis user's manual version 6.12. Dassault Systemes Simulia. Providence, RI, USA
- ALA (American Lifelines Alliance) (2001) Seismic fragility formulations for water systems. Part 1- Guidelines. ASCE-FEMA, Washington, DC, USA.
- ArcelorMittal (2018) High yield SAW welded Pipe API 5L grade X65 PSL 2. 65:5-6.
- Argyroudis S, Pitilakis K (2012) Seismic fragility curves of shallow tunnels in alluvial deposits. *Soil Dyn Earthq Eng*, 23:1-12
- Argyroudis S, Tsinidis G, Gatti F, Pitilakis K (2017) Effects of SSI and lining corrosion on the seismic vulnerability of shallow circular tunnels. *Soil Dyn Earthq Eng*, 98:244-256
- Bai Q, Bai Y (2014) Subsea pipeline design, analysis, and installation. Elsevier, Amsterdam
- Bai Y (2001) Pipelines and risers. Vol. 3. Elsevier, Amsterdam
- Barenberg ME (1988) Correlation of pipeline damage with ground motions. *J Geotech Eng, ASCE*, 114(6):706-711
- Chen WW, Shih BJ, Wu CW, Chen YC (2000) Natural gas pipeline system damages in the Ji-Ji earthquake (The City of Nantou). In: *Proc of the 6th international conf on seismic zonation, USA*
- Darendeli M (2001) Development of a new family of normalized modulus reduction and material damping curves. Ph.D. Dissertation, University of Texas, Austin, USA
- Demirci HE, Bhattacharya S, Karamitros D, Alexander N (2018) Experimental and numerical modelling of buried pipelines crossing reverse faults. *Soil Dyn Earthq Eng* 114:198-214
- Eidinger J (1998) Water distribution system. In: AJ. Schiff (ed) *The Loma Prieta, California, Earthquake of October 17, 1998– Lifelines*. USGS Professional Paper 1552-A, US Government Printing Office, Washington.
- Eidinger J, Maison B, Lee D, Lau B (1995) East Bay municipal district water distribution damage in 1989 Loma Prieta earthquake. *Proceedings of the 4th US Conference on Lifeline Earthquake Engineering, ASCE, TCLEE, Monograph 6*, 240-24.
- El Hmadi K, O'Rourke M (1988) Soil springs for buried pipeline axial motion. *J Geotech Eng*, 114(11):1335-1339
- Elnashai AS, Di Sarno L (2015) *Fundamentals of earthquake engineering. From source to fragility*. Wiley and Sons, UK.
- EQE summary report (1995) The January 17. 1995 Kobe earthquake. EQE International
- European Committee for Standardization (CEN) (2004) EN 1998-1 Eurocode 8: Design of structures for earthquake resistance. Part 1: General Rules, Seismic Actions and Rules for Buildings, European Committee for Standardization, Brussels, Belgium
- European Committee for Standardization (CEN) (2006) EN 1998-4: 2006. Eurocode 8: Design of structures for earthquake resistance. Part 4: Silos, tanks and pipelines. European Committee for Standardization, Brussels, Belgium
- Fotopoulou S, Pitilakis K (2015) Predictive relationships for seismically induced slope displacements using numerical analysis results. *Bull Earthq Eng* 13(11):3207-3238
- Gehl P, Desramaut N, Reveillere A, Modaressi H (2014) Fragility functions of gas and oil networks. SYNER-G: Typology definition and fragility functions for physical elements at seismic risk, *Geotechnical, Geological and Earthquake Engineering, Springer* 27: 187-220.
- Giardini et al. (2013) Seismic Hazard Harmonization in Europe (SHARE): Online Data Resource, doi: 10.12686/SED-00000001-SHARE (last assessed 26.01.2019)

- 1 Hashash YMA, Park D (2002) Viscous damping formulation and high frequency motion propagation in
2 non-linear site response analysis. *Soil Dyn Earthq Eng* 22(7):611-624
- 3 Hashash YMA, Musgrove MI, Harmon JA, Groholski DR, Phillips CA, Park D (2016) DEEPSOIL 6.1,
4 User Manual. USA
- 5 Honegger DG, Gailing RW, Nyman DJ (2002) Guidelines for the seismic design and assessment of
6 natural gas and liquid hydrocarbon pipelines. In the 4th International Pipeline Conference.
7 American Society of Mechanical Engineers, 563-570.
- 8 Housner GW, Jennings PC (1972) The San Fernando California earthquake. *Earthq Eng Struct Dyn* 1:
9 5-31
- 10 Jahangiri V, Shakib H (2018) Seismic risk assessment of buried steel gas pipelines under seismic wave
11 propagation based on fragility analysis. *Bull Earthq Eng* 16(3):1571-1605
- 12 Jeon SS, O'Rourke TD (2005) Northridge earthquake effects on pipelines and residential buildings.
13 *Bull Seismological Soc America*. 95:294-318
- 14 JGA (Japan Gas Association) (2004). Seismic design for gas pipelines, JG(G)-206-03, 91-100.
- 15 Karamitros D, Zoupanitis C, Bouckovalas GD (2016) Buried pipelines with bends: analytical
16 verification against permanent ground displacements. *Can Geotech J* 53(11):1782-1793
- 17 Karamitros DK, Bouckovalas GD, Kourtzis GP (2007) Stress analysis of buried steel pipelines at
18 strike-slip fault crossings. *Soil Dyn Earthq Eng* 27:200-211
- 19 Kyriakides S, Corona E (2007) Plastic buckling and collapse under axial compression. *Mechanical*
20 *Offshore Pipelines Buckling Collapse*, Vol. I, Elsevier Science, New York, 280-318
- 21 Lanzano G, Salzano E, Santucci de Magistris F, Fabbrocino G (2013) Seismic vulnerability of natural
22 gas pipelines. *Reliability Eng System Safety*. 117:73-80
- 23 Lanzano G, Salzano E, Santucci de Magistris F, Fabbrocino G (2014) Seismic vulnerability of gas and
24 liquid buried pipelines. *J Loss Prevention Process Industries* 28:72-78
- 25 Lanzano G, Salzano E, Santucci de Magistris F, Fabbrocino G (2015) Seismic damage to pipelines in
26 the framework of Na-Tech risk assessment. *J Loss Prevention Process Industries* 33:159-172.
- 27 Lee DH, Kim BH, Jeong SH, Jeon JS, Lee TH (2016) Seismic fragility analysis of a buried gas pipeline
28 based on nonlinear time-history analysis. *Inter J Steel Struct* 16(1):231-242
- 29 Lee D-H, Kim BH, Lee H, Kong JS (2009) Seismic behavior of a buried gas pipeline under earthquake
30 excitations. *Eng Struct*, 31:1011-1023
- 31 Melissianos V, Lignos X, Bachas KK, Gantes C (2017b) Experimental investigation of pipes with
32 flexible joints under fault rupture. *J Construct Steel Res* 128:633-648
- 33 Melissianos V, Vamvatsikos D, Gantes C (2017a) Performance-based assessment of protection
34 measures for buried pipes at strike-slip fault crossings. *Soil Dyn Earthq Eng*, 101:1-11
- 35 Melissianos V, Vamvatsikos D, Gantes C (2017c) Performance assessment of buried pipelines at fault
36 crossings. *Earthq Spectra* 33(1):201-218
- 37 Mohareb ME (1995) Deformational behaviour of line pipe, PhD Dissertation, University of Alberta,
38 USA
- 39 NASA (1968) Bucking of thin walled circular cylinders. NASA SP-8007, doi:19690013955
- 40 National Institute of Building Science (NIBS) (2004) Earthquake loss estimation methodology. HAZUS
41 technical manual, Federal Emergency Management Agency (FEMA), Washington, USA.
- 42 Nazemi N, Das S (2010) Behavior of X60 line pipe subjected to axial and lateral deformations. *J*
43 *Pressure Vessel Tech* 132:031701
- 44 O'Rourke MJ (2009) Wave propagation damage to continuous pipe. Technical Council Lifeline
45 Earthquake Engineering Conference (TCLEE), Oakland, CA, June 28-July 1, Reston, VA,
46 American Society of Civil Engineers, USA

- 1 O'Rourke MJ, Ayala G (1993) Pipeline damage due to wave propagation. *J Geotech Eng* 119(9):1490-
2 1498
- 3 O'Rourke MJ, Deyoe E (2004) Seismic damage to segment buried pipe. *Earthq Spectra*
4 20(4):1167-1183
- 5 O'Rourke MJ, Hmadi K (1988) Analysis of continuous buried pipelines for seismic wave effects.
6 *Earthq Eng Struct Dyn* 16:917-929.
- 7 O'Rourke MJ, Liu X (1999) Response of buried pipelines subjected to earthquake effects. University of
8 Buffalo, USA
- 9 O'Rourke TD, Palmer MC (1994) The Northridge, California Earthquake of January 17, 1994:
10 Performance of gas transmission pipelines. Technical Report NCEER-94-0011. National Center for
11 Earthquake Engineering Research. State University of New York at Buffalo, USA
- 12 Paolucci R, Ptilakis K (2007) Seismic risk assessment of underground structures under transient
13 ground deformations. Ptilakis K (ed) *Earthquake Geotechnical Engineering*. Geotechnical,
14 Geological and Earthquake Engineering, Springer, 433-459
- 15 Paquette JA, Kyriakides S (2006) Plastic buckling of tubes under axial compression and internal
16 pressure. *Inter J Mech Sciences* 48:855-867
- 17 Pineda-Porras O, Ordaz M (2003) Seismic vulnerability function for high diameter buried pipelines:
18 Mexico City's primary water system case. *Proceedings of the International Conference on Pipeline*
19 *Engineering Constructions*, 2:1145-1154
- 20 Psyras N, Kwon O, Gerasimidis S, Sextos A (2019) Can a buried gas pipeline experience local
21 buckling during earthquake ground shaking? *Soil Dyn Earthq Eng* 116:511-529
- 22 Psyras N, Sextos A (2018) Safety of buried steel natural gas pipelines under earthquake-induced
23 ground shaking. A review. *Soil Dynamics and Earthquake Engineering*. 106, 254-277
- 24 Sarvanis GC, Karamanos SA, Vazouras P, Mecozzi E, Lucci A, Dakoulas P (2018) Permanent
25 earthquake-induced actions in buried pipelines: Numerical modeling and experimental verification.
26 *Earthq Eng Struct Dyn* 47(4): 966-987
- 27 Scawthorn C, Yanev PI (1995) Preliminary report 17 January 1995, Hyogo-ken Nambu, Japan
28 earthquake. *Eng Struct*, 17(3):146-157
- 29 Seed HB, Idriss IM (1970) Soil moduli and damping factors for dynamic response analyses. College of
30 Engineering, University of California, Berkeley, California
- 31 Timoshenko SP, Gere JM (1961) *Theory of elastic stability*. McGraw-Hill
- 32 Tsatsis A, Gelagoti F, Gazetas G (2018) Performance of a buried pipeline along the dip of a slope
33 experiencing accidental sliding. *Géotechnique* 68:11:968-988
- 34 Tsinidis G, Di Sarno L, Sextos A, Furtner P (2019a) A critical review on the vulnerability assessment of
35 natural gas pipelines subjected to seismic wave propagation. Part 1: Fragility relations and
36 implemented seismic intensity measures. *Tunnelling and Underground Space Technology*, 86:279-
37 296.
- 38 Tsinidis G, Di Sarno L, Sextos A, Psyras N, Furtner P (2018) On the numerical simulation of the
39 response of gas pipelines under compression. In *proceedings of the 9th International Conference on*
40 *Advances in Steel Structures, ICASS'2018*, 5-7 Dec 2018, Hong Kong, China
- 41 Tsinidis G, Di Sarno L, Sextos A, Furtner P (2019b) A critical review on the vulnerability assessment
42 of natural gas pipelines subjected to seismic wave propagation. Part 2: Pipe analysis aspects.
43 *Tunnelling and Underground Space Technology*, 92,103056.
- 44 Vazouras P, Karamanos SA, Dakoulas P (2010) Finite element analysis of buried steel pipelines under
45 strike-slip fault displacements. *Soil Dyn Earthq Eng* 30:1361-1376

- 1 Vazouras P, Karamanos SA, Dakoulas P (2012) Mechanical behavior of buried steel pipes crossing
- 2 active strike-slip faults. Soil Dyn Earthq Eng 41:164-180
- 3 Vazouras P, Karamanos SA, Dakoulas P (2015) Pipe-soil interaction and pipeline performance under
- 4 strike-slip fault movements. Soil Dyn Earthq Eng 72:48-65
- 5 Vazouras P, Karamanos SA (2017) Structural behavior of buried pipe bends and their effect on pipeline
- 6 response in fault crossing areas. Bull Earthq Eng 15(11):4999-5024
- 7 Yun H, Kyriakides S (1990) On the beam and shell modes of buckling of buried pipelines. Soil Dyn
- 8 Earthq Eng 9:179-193.

11 **Appendix A**

12 A series of tables, summarizing the parameters required for the definition of the fragility curves
13 developed in the framework of this study, i.e. the median peak ground velocities corresponding to the
14 limit states, $PGV_{m,i}$ and total lognormal standard deviation β_{tot} , are summarized in this appendix.

Table A1 Median peak ground velocities corresponding to the limit states, $PGV_{m,i}$, and total lognormal standard deviation, β_{tot} , for 406.4 mm pipelines embedded in soil deposit of depth $H = 30$ m (- : the limit state is not reached).

Soil	Steel Grade	Burial depth, h (m)	Cohesive soil deposit – Trench type TA					Cohesionless soil deposit – Trench type TA				
			$PGV_{m,OLS}$ (m/s)	$PGV_{m,PILS}$ (m/s)	$PGV_{m,ULS}$ (m/s)	$PGV_{m,GLS}$ (m/s)	β_{tot}	$PGV_{m,OLS}$ (m/s)	$PGV_{m,PILS}$ (m/s)	$PGV_{m,ULS}$ (m/s)	$PGV_{m,GLS}$ (m/s)	β_{tot}
A-B	X60	1	0.458	2.840	-	-	0.773	1.133	3.199	-	-	0.769
A-B	X65	1	1.167	3.407	-	-	0.749	1.303	3.955	-	-	0.740
A-B	X70	1	1.278	3.915	-	-	0.725	1.424	4.527	-	-	0.717
A-B	X60	2	1.952	-	-	-	0.642	2.274	-	-	-	0.631
A-B	X65	2	2.045	-	-	-	0.659	2.339	-	-	-	0.650
A-B	X70	2	2.341	-	-	-	0.625	2.681	-	-	-	0.615
A-C	X60	1	1.070	3.101	-	-	0.758	1.016	3.154	-	-	0.761
A-C	X65	1	1.240	3.886	-	-	0.734	1.284	4.049	-	-	0.725
A-C	X70	1	1.371	4.529	-	-	0.711	1.374	4.220	-	-	0.676
A-C	X60	2	2.175	-	-	-	0.629	2.296	-	-	-	0.623
A-C	X65	2	2.288	-	-	-	0.649	2.388	-	-	-	0.644
A-C	X70	2	2.647	-	-	-	0.612	2.750	-	-	-	0.607
B-C	X60	1	4.315	-	-	-	0.621	4.655	-	-	-	0.606
B-C	X65	1	4.296	-	-	-	0.612	-	-	-	-	-
B-C	X70	1	4.691	-	-	-	0.601	-	-	-	-	-
B-C	X60	2	-	-	-	-	-	-	-	-	-	-
B-C	X65	2	-	-	-	-	-	-	-	-	-	-
B-C	X70	2	-	-	-	-	-	-	-	-	-	-
Soil	Steel Grade	h (m)	Cohesive soil deposit – Trench type TB					Cohesionless soil deposit – Trench type TB				
			$PGV_{m,OLS}$ (m/s)	$PGV_{m,PILS}$ (m/s)	$PGV_{m,ULS}$ (m/s)	$PGV_{m,GLS}$ (m/s)	β_{tot}	$PGV_{m,OLS}$ (m/s)	$PGV_{m,PILS}$ (m/s)	$PGV_{m,ULS}$ (m/s)	$PGV_{m,GLS}$ (m/s)	β_{tot}
A-B	X60	1	0.458	0.913	1.411	1.711	0.961	0.488	0.990	1.546	1.882	0.995
A-B	X65	1	0.516	1.031	1.596	1.936	0.973	0.518	1.079	1.714	2.103	1.019
A-B	X70	1	0.505	1.048	1.661	2.036	1.020	0.558	1.205	1.959	2.428	1.027
A-B	X60	2	0.486	0.990	1.551	1.892	1.114	0.551	1.197	1.953	2.426	1.085
A-B	X65	2	0.544	1.176	1.913	2.372	1.112	0.625	1.452	2.470	3.125	1.067
A-B	X70	2	0.621	1.445	2.461	3.114	1.066	0.715	1.791	3.194	4.125	1.009
A-C	X60	1	0.432	0.862	1.333	1.616	0.969	0.447	0.900	1.399	1.701	0.968
A-C	X65	1	0.449	0.911	1.422	1.731	1.011	0.473	0.978	1.544	1.891	0.999
A-C	X70	1	0.492	1.047	1.686	2.081	1.011	0.520	1.129	1.840	2.284	0.994
A-C	X60	2	0.482	1.019	1.632	2.011	1.088	0.512	1.118	1.830	2.275	1.055
A-C	X65	2	0.549	1.243	2.082	2.615	1.078	0.586	1.377	2.358	2.992	1.038
A-C	X70	2	0.568	1.252	2.062	2.571	1.077	0.603	1.370	2.299	2.891	1.045
B-C	X60	1	1.290	3.727	-	-	0.812	1.414	4.231	-	-	0.765
B-C	X65	1	1.305	3.780	-	-	0.811	1.709	-	-	-	0.767
B-C	X70	1	1.455	4.447	-	-	0.786	1.591	4.657	-	-	0.713
B-C	X60	2	1.440	4.427	-	-	0.834	2.047	-	-	-	0.749
B-C	X65	2	1.652	-	-	-	0.812	2.407	-	-	-	0.718
B-C	X70	2	1.908	-	-	-	0.770	2.845	-	-	-	0.671

Table A2 Median peak ground velocity corresponding to the limit states, $PGV_{m,i}$ and total lognormal standard deviation β_{tot} for 406.4 mm pipelines embedded in soil deposit of depth $H = 60$ m (- : the limit state is not reached).

Soil	Steel Grade	Burial depth, h (m)	Cohesive soil deposit – Trench type TA					Cohesionless soil deposit – Trench type TA				
			$PGV_{m,OLS}$ (m/s)	$PGV_{m,PILS}$ (m/s)	$PGV_{m,ULS}$ (m/s)	$PGV_{m,GLS}$ (m/s)	β_{tot}	$PGV_{m,OLS}$ (m/s)	$PGV_{m,PILS}$ (m/s)	$PGV_{m,ULS}$ (m/s)	$PGV_{m,GLS}$ (m/s)	β_{tot}
A-B	X60	1	0.809	2.176	4.059	-	0.741	0.902	2.482	4.700	-	0.755
A-B	X65	1	0.924	2.660	-	-	0.719	1.013	2.949	-	-	0.724
A-B	X70	1	1.044	3.212	-	-	0.697	1.069	3.187	-	-	0.731
A-B	X60	2	1.525	-	-	-	0.634	1.811	-	-	-	0.630
A-B	X65	2	1.781	-	-	-	0.621	1.811	-	-	-	0.662
A-B	X70	2	2.081	-	-	-	0.593	2.144	-	-	-	0.618
A-C	X60	1	0.700	1.749	3.117	4.024	0.742	0.742	1.878	3.374	4.372	0.758
A-C	X65	1	0.791	2.106	3.904	-	0.723	0.845	2.287	4.286	-	0.738
A-C	X70	1	0.877	2.468	4.739	-	0.705	0.952	2.752	-	-	0.717
A-C	X60	2	1.245	4.194	-	-	0.646	1.376	4.867	-	-	0.652
A-C	X65	2	1.495	-	-	-	0.623	1.595	-	-	-	0.641
A-C	X70	2	1.744	-	-	-	0.598	1.859	-	-	-	0.610
B-C	X60	1	1.533	4.740	-	-	0.741	1.775	-	-	-	0.703
B-C	X65	1	1.724	-	-	-	0.700	2.172	-	-	-	0.674
B-C	X70	1	1.810	-	-	-	0.687	2.399	-	-	-	0.646
B-C	X60	2	2.895	-	-	-	0.611	3.422	-	-	-	0.614
B-C	X65	2	3.711	-	-	-	0.592	4.016	-	-	-	0.590
B-C	X70	2	3.711	-	-	-	0.577	4.588	-	-	-	0.575
Soil	Steel Grade	h (m)	Cohesive soil deposit – Trench type TB					Cohesionless soil deposit – Trench type TB				
			$PGV_{m,OLS}$ (m/s)	$PGV_{m,PILS}$ (m/s)	$PGV_{m,ULS}$ (m/s)	$PGV_{m,GLS}$ (m/s)	β_{tot}	$PGV_{m,OLS}$ (m/s)	$PGV_{m,PILS}$ (m/s)	$PGV_{m,ULS}$ (m/s)	$PGV_{m,GLS}$ (m/s)	β_{tot}
A-B	X60	1	0.345	0.647	0.961	1.145	0.903	0.380	0.727	1.094	1.310	0.870
A-B	X65	1	0.354	0.665	0.989	1.180	0.935	0.396	0.766	1.162	1.397	0.892
A-B	X70	1	0.376	0.725	1.098	1.319	0.952	0.423	0.847	1.310	1.590	0.911
A-B	X60	2	0.366	0.697	1.048	1.255	1.051	0.410	0.816	1.260	1.526	1.008
A-B	X65	2	0.400	0.795	1.227	1.487	1.061	0.456	0.958	1.530	1.883	0.998
A-B	X70	2	0.439	0.918	1.462	1.796	1.059	0.522	1.183	1.983	2.492	0.964
A-C	X60	1	0.432	0.862	1.333	1.616	0.938	0.336	0.607	0.883	1.042	0.927
A-C	X65	1	0.324	0.578	0.833	0.979	0.961	0.341	0.616	0.893	1.053	0.960
A-C	X70	1	0.340	0.620	0.906	1.072	0.972	0.359	0.665	0.981	1.165	0.964
A-C	X60	2	0.330	0.591	0.854	1.005	1.070	0.351	0.652	0.962	1.143	1.045
A-C	X65	2	0.353	0.654	0.965	1.146	1.090	0.387	0.754	1.148	1.383	1.032
A-C	X70	2	0.389	0.760	1.158	1.395	1.080	0.427	0.880	1.387	1.696	1.018
B-C	X60	1	0.689	1.599	2.721	3.442	0.936	0.801	1.961	3.449	4.428	0.900
B-C	X65	1	0.733	1.744	3.014	3.839	0.956	0.828	2.055	3.644	4.696	0.929
B-C	X70	1	0.796	1.978	3.511	4.526	0.930	0.874	2.220	3.998	-	0.917
B-C	X60	2	0.796	1.989	3.544	4.575	0.985	0.809	1.984	3.492	4.485	1.003
B-C	X65	2	0.843	2.157	3.901	-	0.986	0.891	2.294	4.164	-	0.978
B-C	X70	2	0.966	2.663	-	-	0.920	1.000	2.736	-	-	0.924

Table A3 Median peak ground velocity corresponding to the limit states, $PGV_{m,i}$, and total lognormal standard deviation, β_{tot} , for 406.4 mm pipelines embedded in soil deposit of depth $H = 120$ m (- : the limit state is not reached).

Soil	Steel Grade	Burial depth, h (m)	Cohesive soil deposit – Trench type TA					Cohesionless soil deposit – Trench type TA				
			$PGV_{m,OLS}$ (m/s)	$PGV_{m,PILS}$ (m/s)	$PGV_{m,ULS}$ (m/s)	$PGV_{m,GLS}$ (m/s)	β_{tot}	$PGV_{m,OLS}$ (m/s)	$PGV_{m,PILS}$ (m/s)	$PGV_{m,ULS}$ (m/s)	$PGV_{m,GLS}$ (m/s)	β_{tot}
A-B	X60	1	0.548	1.390	2.498	3.239	0.718	0.613	1.526	2.710	3.495	0.712
A-B	X65	1	0.591	1.549	2.842	3.718	0.721	0.680	1.784	3.275	4.286	0.691
A-B	X70	1	0.657	1.817	3.451	4.584	0.702	0.757	2.104	4.006	-	0.669
A-B	X60	2	0.958	3.226	-	-	0.642	1.145	4.013	-	-	0.615
A-B	X65	2	1.169	4.389	-	-	0.605	1.396	-	-	-	0.591
A-B	X70	2	1.274	4.994	-	-	0.622	1.493	-	-	-	0.608
A-C	X60	1	0.454	1.062	1.813	2.298	0.747	0.497	1.147	1.941	2.450	0.726
A-C	X65	1	0.498	1.219	2.141	2.748	0.737	0.547	1.322	2.307	2.951	0.714
A-C	X70	1	0.549	1.415	2.570	3.346	0.715	0.603	1.538	2.773	3.600	0.688
A-C	X60	2	0.764	2.338	4.731	-	0.655	0.852	2.635	-	-	0.625
A-C	X65	2	0.907	3.042	-	-	0.623	1.596	-	-	-	0.608
A-C	X70	2	1.049	3.816	-	-	0.598	1.170	4.302	-	-	0.583
B-C	X60	1	1.208	3.868	-	-	0.704	1.463	4.406	-	-	0.673
B-C	X65	1	1.395	4.796	-	-	0.677	1.640	-	-	-	0.663
B-C	X70	1	1.417	4.890	-	-	0.696	1.812	-	-	-	0.653
B-C	X60	2	2.519	-	-	-	0.590	2.751	-	-	-	0.611
B-C	X65	2	2.630	-	-	-	0.608	3.092	-	-	-	0.600
B-C	X70	2	2.863	-	-	-	0.593	2.940	-	-	-	0.616
Soil	Steel Grade	h (m)	Cohesive soil deposit – Trench type TB					Cohesionless soil deposit – Trench type TB				
			$PGV_{m,OLS}$ (m/s)	$PGV_{m,PILS}$ (m/s)	$PGV_{m,ULS}$ (m/s)	$PGV_{m,GLS}$ (m/s)	β_{tot}	$PGV_{m,OLS}$ (m/s)	$PGV_{m,PILS}$ (m/s)	$PGV_{m,ULS}$ (m/s)	$PGV_{m,GLS}$ (m/s)	β_{tot}
A-B	X60	1	0.267	0.480	0.694	0.818	0.997	0.303	0.542	0.782	0.920	0.992
A-B	X65	1	0.274	0.494	0.716	0.843	1.034	0.312	0.559	0.807	0.950	1.037
A-B	X70	1	0.288	0.530	0.778	0.923	1.039	0.331	0.610	0.897	1.063	1.037
A-B	X60	2	0.279	0.502	0.726	0.855	1.145	0.317	0.574	0.836	0.987	1.131
A-B	X65	2	0.296	0.546	0.803	0.952	1.158	0.343	0.647	0.964	1.150	1.130
A-B	X70	2	0.325	0.629	0.953	1.146	1.124	0.375	0.740	1.135	1.372	1.097
A-C	X60	1	0.246	0.432	0.615	0.719	1.012	0.269	0.464	0.655	0.763	0.998
A-C	X65	1	0.250	0.436	0.618	0.721	1.031	0.273	0.470	0.661	0.769	1.036
A-C	X70	1	0.262	0.465	0.666	0.782	1.046	0.286	0.501	0.713	0.834	1.051
A-C	X60	2	0.255	0.442	0.626	0.729	1.166	0.273	0.470	0.661	0.769	1.179
A-C	X65	2	0.268	0.472	0.675	0.790	1.206	0.289	0.508	0.726	0.850	1.206
A-C	X70	2	0.288	0.526	0.768	0.908	1.194	0.313	0.571	0.836	0.989	1.193
B-C	X60	1	0.498	1.111	1.844	2.308	0.905	0.614	1.453	2.501	3.180	0.841
B-C	X65	1	0.543	1.255	2.128	2.688	0.933	0.656	1.613	2.844	3.656	0.867
B-C	X70	1	0.601	1.464	2.566	3.289	0.919	0.743	1.954	3.595	4.708	0.841
B-C	X60	2	0.590	1.429	2.494	3.192	0.991	0.728	1.910	3.507	4.589	0.889
B-C	X65	2	0.678	1.766	3.228	4.216	0.960	0.866	2.491	4.849	-	0.840
B-C	X70	2	0.812	2.340	4.560	-	0.887	1.036	3.295	-	-	0.802

Table A4 Median peak ground velocity corresponding to the limit states, $PGV_{m,i}$, and total lognormal standard deviation, β_{tot} , for 508.0 mm pipelines embedded in soil deposit of depth $H = 30$ m (- : the limit state is not reached).

Soil	Steel Grade	Burial depth, h (m)	Cohesive soil deposit – Trench type TA					Cohesionless soil deposit – Trench type TA				
			$PGV_{m,OLS}$ (m/s)	$PGV_{m,PILS}$ (m/s)	$PGV_{m,ULS}$ (m/s)	$PGV_{m,GLS}$ (m/s)	β_{tot}	$PGV_{m,OLS}$ (m/s)	$PGV_{m,PILS}$ (m/s)	$PGV_{m,ULS}$ (m/s)	$PGV_{m,GLS}$ (m/s)	β_{tot}
A-B	X60	1	1.139	3.356	-	-	0.791	0.802	2.336	4.524	-	0.758
A-B	X65	1	0.841	2.648	-	-	0.774	0.901	2.803	-	-	0.738
A-B	X70	1	0.962	3.306	-	-	0.734	1.031	3.503	-	-	0.700
A-B	X60	2	1.535	0.000	-	-	0.628	1.816	-	-	-	0.618
A-B	X65	2	1.895	0.000	-	-	0.599	2.243	-	-	-	0.593
A-B	X70	2	2.201	0.000	-	-	0.581	2.564	-	-	-	0.578
A-C	X60	1	0.752	2.333	4.697	-	0.773	0.798	2.530	-	-	0.761
A-C	X65	1	0.861	2.894	-	-	0.754	0.933	3.244	-	-	0.738
A-C	X70	1	1.001	3.713	-	-	0.714	1.065	4.045	-	-	0.700
A-C	X60	2	1.630	-	-	-	0.619	1.758	-	-	-	0.613
A-C	X65	2	2.044	-	-	-	0.592	2.192	-	-	-	0.589
A-C	X70	2	2.393	-	-	-	0.576	2.475	-	-	-	0.572
B-C	X60	1	2.214	-	-	-	0.711	2.328	-	-	-	0.687
B-C	X65	1	2.155	-	-	-	0.700	3.133	-	-	-	0.671
B-C	X70	1	2.410	-	-	-	0.681	3.537	-	-	-	0.646
B-C	X60	2	2.683	-	-	-	0.625	3.985	-	-	-	0.609
B-C	X65	2	3.670	-	-	-	0.607	4.552	-	-	-	0.597
B-C	X70	2	3.847	-	-	-	0.597	4.918	-	-	-	0.596
Soil	Steel Grade	h (m)	Cohesive soil deposit – Trench type TB					Cohesionless soil deposit – Trench type TB				
			$PGV_{m,OLS}$ (m/s)	$PGV_{m,PILS}$ (m/s)	$PGV_{m,ULS}$ (m/s)	$PGV_{m,GLS}$ (m/s)	β_{tot}	$PGV_{m,OLS}$ (m/s)	$PGV_{m,PILS}$ (m/s)	$PGV_{m,ULS}$ (m/s)	$PGV_{m,GLS}$ (m/s)	β_{tot}
A-B	X60	1	0.328	0.639	0.967	1.319	1.051	0.356	0.693	1.046	1.426	1.019
A-B	X65	1	0.342	0.679	1.038	1.428	1.066	0.373	0.743	1.138	1.567	1.033
A-B	X70	1	0.363	0.750	1.174	1.643	1.053	0.398	0.825	1.295	1.818	1.021
A-B	X60	2	0.486	1.224	2.166	3.326	0.863	0.486	1.224	2.166	3.326	0.863
A-B	X65	2	0.562	1.551	2.906	4.658	0.857	0.742	2.413	-	0.000	0.781
A-B	X70	2	0.954	3.830	-	-	0.635	0.890	3.277	-	0.000	0.726
A-C	X60	1	0.314	0.627	0.960	1.322	1.027	0.329	0.667	1.034	1.437	1.017
A-C	X65	1	0.329	0.667	1.033	1.435	1.045	0.345	0.717	1.126	1.581	1.039
A-C	X70	1	0.350	0.740	1.176	1.665	1.035	0.369	0.800	1.290	1.848	1.026
A-C	X60	2	0.571	1.694	3.320	-	0.732	0.645	2.079	4.287	-	0.697
A-C	X65	2	0.724	2.523	-	-	0.684	0.832	3.178	-	-	0.654
A-C	X70	2	0.920	3.806	-	-	0.640	1.056	4.766	-	-	0.614
B-C	X60	1	0.847	2.480	4.817	-	0.917	0.898	2.714	-	-	0.854
B-C	X65	1	0.717	1.907	3.493	-	0.909	0.987	3.134	-	-	0.847
B-C	X70	1	0.919	2.820	-	-	0.899	1.075	3.596	-	-	0.826
B-C	X60	2	1.188	4.101	-	-	0.879	1.902	-	-	-	0.696
B-C	X65	2	1.375	-	-	-	0.851	2.431	-	-	-	0.660
B-C	X70	2	1.392	-	-	-	0.815	2.715	-	-	-	0.628

Table A5 Median peak ground velocity corresponding to the limit states, $PGV_{m,i}$, and total lognormal standard deviation, β_{tot} , for 508.0 mm pipelines embedded in soil deposit of depth $H = 60$ m (- : the limit state is not reached).

Soil	Steel Grade	Burial depth, h (m)	Cohesive soil deposit – Trench type TA					Cohesionless soil deposit – Trench type TA				
			$PGV_{m,OLS}$ (m/s)	$PGV_{m,PILS}$ (m/s)	$PGV_{m,ULS}$ (m/s)	$PGV_{m,GLS}$ (m/s)	β_{tot}	$PGV_{m,OLS}$ (m/s)	$PGV_{m,PILS}$ (m/s)	$PGV_{m,ULS}$ (m/s)	$PGV_{m,GLS}$ (m/s)	β_{tot}
A-B	X60	1	0.491	1.226	2.158	3.301	0.860	0.548	1.407	2.521	3.907	0.844
A-B	X65	1	0.531	1.381	2.495	3.889	0.879	0.605	1.643	3.047	4.846	0.833
A-B	X70	1	0.962	3.306	-	-	0.734	0.658	1.883	3.606	0.000	0.846
A-B	X60	2	0.956	3.504	-	-	0.693	1.137	4.529	-	-	0.648
A-B	X65	2	1.133	4.594	-	-	0.668	1.283	-	-	-	0.672
A-B	X70	2	1.303	0.000	-	-	0.632	1.629	-	-	-	0.631
A-C	X60	1	0.445	1.044	1.770	2.631	0.864	0.470	1.120	1.915	2.867	0.873
A-C	X65	1	0.472	1.140	1.965	2.959	0.888	0.508	1.247	2.174	3.301	0.861
A-C	X70	1	0.515	1.311	2.338	3.610	0.877	0.554	1.450	2.630	4.113	0.875
A-C	X60	2	0.832	2.803	-	-	0.679	0.964	3.565	-	-	0.655
A-C	X65	2	1.001	3.781	-	-	0.651	1.063	4.150	-	-	0.681
A-C	X70	2	1.157	4.807	-	-	0.628	1.217	-	-	-	0.643
B-C	X60	1	1.013	3.215	-	-	0.802	1.061	3.358	-	-	0.790
B-C	X65	1	1.072	3.513	-	-	0.771	1.223	4.167	-	-	0.800
B-C	X70	1	1.096	3.622	-	-	0.772	1.312	4.655	-	-	0.764
B-C	X60	2	1.880	-	-	-	0.636	2.224	-	-	-	0.658
B-C	X65	2	2.211	-	-	-	0.619	2.690	-	-	-	0.624
B-C	X70	2	2.193	-	-	-	0.652	3.099	-	-	-	0.605
Soil	Steel Grade	h (m)	Cohesive soil deposit – Trench type TB					Cohesionless soil deposit – Trench type TB				
			$PGV_{m,OLS}$ (m/s)	$PGV_{m,PILS}$ (m/s)	$PGV_{m,ULS}$ (m/s)	$PGV_{m,GLS}$ (m/s)	β_{tot}	$PGV_{m,OLS}$ (m/s)	$PGV_{m,PILS}$ (m/s)	$PGV_{m,ULS}$ (m/s)	$PGV_{m,GLS}$ (m/s)	β_{tot}
A-B	X60	1	0.260	0.493	0.733	0.987	0.976	0.275	0.513	0.753	1.005	0.987
A-B	X65	1	0.268	0.506	0.751	1.011	0.994	0.285	0.536	0.791	1.060	1.002
A-B	X70	1	0.281	0.548	0.827	1.126	0.981	0.302	0.587	0.885	1.205	0.984
A-B	X60	2	0.310	0.623	0.960	1.327	0.983	0.328	0.657	1.008	1.392	1.005
A-B	X65	2	0.339	0.714	1.133	1.602	0.985	0.368	0.789	1.264	1.801	1.011
A-B	X70	2	0.381	0.869	1.448	2.124	0.951	0.406	0.929	1.550	2.278	0.961
A-C	X60	1	0.244	0.441	0.636	0.838	0.988	0.258	0.475	0.693	0.921	0.985
A-C	X65	1	0.253	0.460	0.667	0.881	0.994	0.267	0.493	0.722	0.961	0.997
A-C	X70	1	0.264	0.490	0.719	0.959	0.980	0.278	0.527	0.782	1.052	0.977
A-C	X60	2	0.294	0.568	0.853	1.159	0.994	0.305	0.603	0.919	1.261	0.969
A-C	X65	2	0.320	0.649	1.006	1.398	0.968	0.340	0.719	1.142	1.617	0.930
A-C	X70	2	0.352	0.762	1.229	1.760	0.930	0.367	0.812	1.328	1.921	0.914
B-C	X60	1	0.456	1.027	1.699	2.478	1.012	0.508	1.185	2.001	2.966	1.008
B-C	X65	1	0.483	1.115	1.872	2.761	1.033	0.550	1.344	2.337	3.540	1.010
B-C	X70	1	0.522	1.269	2.198	3.322	1.006	0.599	1.551	2.794	4.346	0.973
B-C	X60	2	0.661	1.819	3.401	-	0.967	0.689	1.878	3.490	-	0.979
B-C	X65	2	0.682	1.880	3.521	-	0.984	0.789	2.307	4.481	-	0.947
B-C	X70	2	0.832	2.625	-	-	0.886	0.863	2.696	-	-	0.906

Table A6 Median peak ground velocity corresponding to the limit states, $PGV_{m,i}$, and total lognormal standard deviation, β_{tot} , for 508.0 mm pipelines embedded in soil deposit of depth $H = 120$ m (- : the limit state is not reached).

Soil	Steel Grade	Burial depth, h (m)	Cohesive soil deposit – Trench type TA					Cohesionless soil deposit – Trench type TA				
			$PGV_{m,OLS}$ (m/s)	$PGV_{m,PILS}$ (m/s)	$PGV_{m,ULS}$ (m/s)	$PGV_{m,GLS}$ (m/s)	β_{tot}	$PGV_{m,OLS}$ (m/s)	$PGV_{m,PILS}$ (m/s)	$PGV_{m,ULS}$ (m/s)	$PGV_{m,GLS}$ (m/s)	β_{tot}
A-B	X60	1	0.380	0.904	1.542	2.305	0.893	0.437	1.043	1.786	2.676	0.863
A-B	X65	1	0.405	0.989	1.717	2.599	0.901	0.470	1.163	2.037	3.102	0.861
A-B	X70	1	0.445	1.151	2.072	3.222	0.876	0.518	1.364	2.481	3.889	0.827
A-B	X60	2	0.737	2.566	-	-	0.663	0.860	3.087	-	-	0.646
A-B	X65	2	0.892	3.493	-	-	0.635	1.032	4.142	-	-	0.623
A-B	X70	2	1.044	4.521	-	-	0.609	1.178	-	-	-	0.611
A-C	X60	1	0.290	0.569	0.863	1.181	0.997	0.361	0.785	1.269	1.821	0.927
A-C	X65	1	0.303	0.602	0.922	1.268	1.028	0.380	0.841	1.376	1.991	0.936
A-C	X70	1	0.320	0.654	1.017	1.419	1.024	0.400	0.855	1.370	1.951	0.973
A-C	X60	2	0.601	1.864	3.754	-	0.698	0.623	1.876	3.707	-	0.723
A-C	X65	2	0.697	2.367	-	-	0.668	0.739	2.469	-	-	0.681
A-C	X70	2	0.778	2.819	-	-	0.662	0.881	3.315	-	-	0.640
B-C	X60	1	0.815	2.678	-	-	0.759	0.858	2.718	-	-	0.755
B-C	X65	1	0.890	3.070	-	-	0.746	1.030	3.631	-	-	0.739
B-C	X70	1	0.944	3.351	-	-	0.736	1.071	3.840	-	-	0.749
B-C	X60	2	2.028	-	-	-	0.595	2.063	-	-	-	0.610
B-C	X65	2	2.211	-	-	-	0.619	2.037	-	-	-	0.635
B-C	X70	2	2.037	-	-	-	0.619	2.352	-	-	-	0.609
Soil	Steel Grade	h (m)	Cohesive soil deposit – Trench type TB					Cohesionless soil deposit – Trench type TB				
			$PGV_{m,OLS}$ (m/s)	$PGV_{m,PILS}$ (m/s)	$PGV_{m,ULS}$ (m/s)	$PGV_{m,GLS}$ (m/s)	β_{tot}	$PGV_{m,OLS}$ (m/s)	$PGV_{m,PILS}$ (m/s)	$PGV_{m,ULS}$ (m/s)	$PGV_{m,GLS}$ (m/s)	β_{tot}
A-B	X60	1	0.201	0.363	0.523	0.687	1.081	0.229	0.407	0.581	0.760	1.076
A-B	X65	1	0.210	0.380	0.549	0.723	1.117	0.236	0.419	0.598	0.781	1.117
A-B	X70	1	0.220	0.410	0.601	0.802	1.107	0.246	0.449	0.650	0.858	1.098
A-B	X60	2	0.237	0.443	0.653	0.873	1.129	0.267	0.499	0.733	0.980	1.125
A-B	X65	2	0.255	0.491	0.737	1.001	1.130	0.289	0.561	0.845	1.151	1.135
A-B	X70	2	0.273	0.550	0.848	1.173	1.115	0.309	0.627	0.972	1.350	1.087
A-C	X60	1	0.188	0.328	0.463	0.599	1.087	0.206	0.352	0.491	0.629	1.085
A-C	X65	1	0.193	0.335	0.471	0.608	1.113	0.212	0.361	0.503	0.645	1.117
A-C	X70	1	0.205	0.368	0.528	0.694	1.096	0.223	0.395	0.561	0.731	1.106
A-C	X60	2	0.227	0.421	0.617	0.822	1.119	0.237	0.425	0.610	0.800	1.160
A-C	X65	2	0.230	0.420	0.610	0.807	1.188	0.250	0.457	0.665	0.880	1.190
A-C	X70	2	0.259	0.514	0.785	1.080	1.114	0.273	0.530	0.798	1.086	1.147
B-C	X60	1	0.337	0.729	1.175	1.681	1.012	0.390	0.877	1.448	2.110	0.948
B-C	X65	1	0.350	0.769	1.252	1.804	1.025	0.417	0.969	1.633	2.418	0.958
B-C	X70	1	0.373	0.853	1.422	2.088	1.012	0.450	1.100	1.912	2.897	0.940
B-C	X60	2	0.431	1.037	1.784	2.682	1.029	0.527	1.378	2.498	3.907	0.943
B-C	X65	2	0.487	1.261	2.271	3.534	1.007	0.690	2.019	3.922	-	0.868
B-C	X70	2	0.585	1.700	3.289	-	0.925	0.717	2.300	4.727	-	0.814

Table A7 Median peak ground velocity corresponding to the limit states, $PGV_{m,i}$, and total lognormal standard deviation, β_{tot} , for 762.0 mm pipelines embedded in soil deposit of depth $H = 30$ m (- : the limit state is not reached).

Soil	Steel Grade	Burial depth, h (m)	Cohesive soil deposit – Trench type TA					Cohesionless soil deposit – Trench type TA				
			$PGV_{m,OLS}$ (m/s)	$PGV_{m,PILS}$ (m/s)	$PGV_{m,ULS}$ (m/s)	$PGV_{m,GLS}$ (m/s)	β_{tot}	$PGV_{m,OLS}$ (m/s)	$PGV_{m,PILS}$ (m/s)	$PGV_{m,ULS}$ (m/s)	$PGV_{m,GLS}$ (m/s)	β_{tot}
A-B	X60	1	1.230	3.962	-	-	0.767	1.407	4.789	-	-	0.754
A-B	X65	1	1.321	4.391	-	-	0.772	1.521	-	-	-	0.747
A-B	X70	1	1.656	-	-	-	0.690	1.736	-	-	-	0.708
A-B	X60	2	2.013	-	-	-	0.648	2.333	-	-	-	0.644
A-B	X65	2	2.321	-	-	-	0.637	2.636	-	-	-	0.629
A-B	X70	2	2.685	-	-	-	0.603	3.159	-	-	-	0.597
A-C	X60	1	1.343	4.740	-	-	0.732	1.407	4.789	-	-	0.754
A-C	X65	1	1.471	-	-	-	0.739	1.521	-	-	-	0.747
A-C	X70	1	1.696	-	-	-	0.700	1.736	-	-	-	0.708
A-C	X60	2	2.233	-	-	-	0.637	2.394	-	-	-	0.629
A-C	X65	2	2.561	-	-	-	0.625	2.733	-	-	-	0.616
A-C	X70	2	3.108	-	-	-	0.590	3.159	-	-	-	0.597
B-C	X60	1	-	-	-	-	-	-	-	-	-	-
B-C	X65	1	-	-	-	-	-	-	-	-	-	-
B-C	X70	1	-	-	-	-	-	-	-	-	-	-
B-C	X60	2	-	-	-	-	-	-	-	-	-	-
B-C	X65	2	-	-	-	-	-	-	-	-	-	-
B-C	X70	2	-	-	-	-	-	-	-	-	-	-
Soil	Steel Grade	h (m)	Cohesive soil deposit – Trench type TB					Cohesionless soil deposit – Trench type TB				
			$PGV_{m,OLS}$ (m/s)	$PGV_{m,PILS}$ (m/s)	$PGV_{m,ULS}$ (m/s)	$PGV_{m,GLS}$ (m/s)	β_{tot}	$PGV_{m,OLS}$ (m/s)	$PGV_{m,PILS}$ (m/s)	$PGV_{m,ULS}$ (m/s)	$PGV_{m,GLS}$ (m/s)	β_{tot}
A-B	X60	1	0.649	1.711	3.118	4.609	0.989	0.574	1.350	2.291	3.233	1.030
A-B	X65	1	0.557	1.297	2.188	3.075	1.079	0.628	1.552	2.715	3.908	1.034
A-B	X70	1	0.612	1.507	2.632	3.784	1.052	0.696	1.828	3.321	4.900	0.993
A-B	X60	2	0.515	1.295	2.293	3.326	1.067	0.664	1.744	3.169	4.677	1.010
A-B	X65	2	0.648	1.683	3.035	4.457	1.059	0.783	2.275	4.400	-	0.986
A-B	X70	2	0.722	2.005	3.770	-	1.013	0.855	2.623	-	-	0.927
A-C	X60	1	0.513	1.195	2.015	2.834	1.015	0.529	1.238	2.095	2.951	1.020
A-C	X65	1	0.566	1.393	2.432	3.496	1.030	0.597	1.502	2.658	3.854	1.005
A-C	X70	1	0.616	1.591	2.862	4.195	1.021	0.649	1.711	3.118	4.609	0.989
A-C	X60	2	0.618	1.627	2.962	4.377	1.022	0.685	1.697	2.973	4.284	1.032
A-C	X65	2	0.685	1.932	3.670	-	1.011	0.736	2.172	4.241	-	0.968
A-C	X70	2	0.786	2.425	4.867	-	0.947	0.883	2.929	-	-	0.897
B-C	X60	1	1.484	-	-	-	0.818	2.008	-	-	-	0.751
B-C	X65	1	1.831	-	-	-	0.806	2.270	-	-	-	0.734
B-C	X70	1	2.039	-	-	-	0.784	2.611	-	-	-	0.701
B-C	X60	2	1.922	-	-	-	0.804	2.680	-	-	-	0.697
B-C	X65	2	2.505	-	-	-	0.747	3.004	-	-	-	0.670
B-C	X70	2	2.375	-	-	-	0.747	3.744	-	-	-	0.628

Table A8. Median peak ground velocity corresponding to the limit states, $PGV_{m,i}$, and total lognormal standard deviation, β_{tot} , for 762.0 mm pipelines embedded in soil deposit of depth $H = 60$ m (- : the limit state is not reached).

Soil	Steel Grade	Burial depth, h (m)	Cohesive soil deposit – Trench type TA					Cohesionless soil deposit – Trench type TA				
			$PGV_{m,OLS}$ (m/s)	$PGV_{m,PILS}$ (m/s)	$PGV_{m,ULS}$ (m/s)	$PGV_{m,GLS}$ (m/s)	β_{tot}	$PGV_{m,OLS}$ (m/s)	$PGV_{m,PILS}$ (m/s)	$PGV_{m,ULS}$ (m/s)	$PGV_{m,GLS}$ (m/s)	β_{tot}
A-B	X60	1	0.921	2.827	-	-	0.772	1.034	3.259	-	-	0.778
A-B	X65	1	1.101	3.732	-	-	0.741	1.180	3.988	-	-	0.755
A-B	X70	1	1.656	-	-	-	0.712	1.431	-	-	-	0.719
A-B	X60	2	1.474	-	-	-	0.649	1.824	-	-	-	0.629
A-B	X65	2	1.890	-	-	-	0.611	2.331	-	-	-	0.602
A-B	X70	2	2.235	-	-	-	0.593	2.403	-	-	-	0.610
A-C	X60	1	0.774	2.158	4.069	-	0.795	0.832	2.370	4.530	-	0.792
A-C	X65	1	0.889	2.675	-	-	0.771	0.985	3.089	-	-	0.760
A-C	X70	1	1.066	3.568	-	-	0.712	1.160	4.005	-	-	0.717
A-C	X60	2	1.304	-	-	-	0.645	1.324	-	-	-	0.667
A-C	X65	2	1.470	-	-	-	0.642	1.683	-	-	-	0.626
A-C	X70	2	1.831	-	-	-	0.598	1.970	-	-	-	0.608
B-C	X60	1	1.995	-	-	-	0.720	2.071	-	-	-	0.724
B-C	X65	1	1.873	-	-	-	0.735	2.664	-	-	-	0.702
B-C	X70	1	2.280	-	-	-	0.684	2.887	-	-	-	0.673
B-C	X60	2	3.177	-	-	-	0.615	4.127	-	-	-	0.611
B-C	X65	2	3.552	-	-	-	0.603	4.956	-	-	-	0.592
B-C	X70	2	4.083	-	-	-	0.588	-	-	-	-	-
Soil	Steel Grade	h (m)	Cohesive soil deposit – Trench type TB					Cohesionless soil deposit – Trench type TB				
			$PGV_{m,OLS}$ (m/s)	$PGV_{m,PILS}$ (m/s)	$PGV_{m,ULS}$ (m/s)	$PGV_{m,GLS}$ (m/s)	β_{tot}	$PGV_{m,OLS}$ (m/s)	$PGV_{m,PILS}$ (m/s)	$PGV_{m,ULS}$ (m/s)	$PGV_{m,GLS}$ (m/s)	β_{tot}
A-B	X60	1	0.375	0.763	1.183	1.575	1.035	0.431	0.922	1.477	2.007	0.982
A-B	X65	1	0.404	0.854	1.357	1.835	1.048	0.461	1.021	1.668	2.296	1.019
A-B	X70	1	0.424	0.919	1.482	2.024	1.093	0.499	1.154	1.940	2.721	1.042
A-B	X60	2	0.413	0.897	1.449	1.980	1.084	0.472	1.089	1.826	2.559	1.029
A-B	X65	2	0.477	1.131	1.929	2.731	1.032	0.596	1.606	2.963	4.416	0.935
A-B	X70	2	0.525	1.321	2.338	3.392	1.057	0.652	1.853	3.534	-	0.926
A-C	X60	1	0.338	0.645	0.961	1.246	1.052	0.367	0.725	1.104	1.452	1.008
A-C	X65	1	0.359	0.703	1.064	1.395	1.076	0.389	0.786	1.215	1.614	1.044
A-C	X70	1	0.383	0.778	1.206	1.604	1.089	0.419	0.886	1.406	1.901	1.061
A-C	X60	2	0.380	0.786	1.233	1.653	1.094	0.395	0.830	1.315	1.774	1.071
A-C	X65	2	0.403	0.855	1.362	1.843	1.119	0.456	1.049	1.754	2.453	1.045
A-C	X70	2	0.428	0.941	1.530	2.101	1.141	0.524	1.320	2.338	3.393	1.012
B-C	X60	1	0.791	2.125	3.916	-	0.946	0.866	2.370	4.417	-	0.953
B-C	X65	1	0.874	2.480	4.727	-	0.923	0.892	2.458	4.602	-	0.975
B-C	X70	1	0.961	2.879	-	-	0.893	0.910	2.526	4.750	-	0.971
B-C	X60	2	0.888	2.589	-	-	0.950	0.988	2.985	-	-	0.916
B-C	X65	2	1.074	3.513	-	-	0.886	1.181	3.934	-	-	0.871
B-C	X70	2	1.239	4.413	-	-	0.854	1.121	3.614	-	-	0.914

Table A9. Median peak ground velocity corresponding to the limit states, $PGV_{m,i}$, and total lognormal standard deviation, β_{tot} , for 762.0 mm pipelines embedded in soil deposit of depth $H = 120$ m (- : the limit state is not reached).

Soil	Steel Grade	Burial depth, h (m)	Cohesive soil deposit – Trench type TA					Cohesionless soil deposit – Trench type TA				
			$PGV_{m,OLS}$ (m/s)	$PGV_{m,PILS}$ (m/s)	$PGV_{m,ULS}$ (m/s)	$PGV_{m,GLS}$ (m/s)	β_{tot}	$PGV_{m,OLS}$ (m/s)	$PGV_{m,PILS}$ (m/s)	$PGV_{m,ULS}$ (m/s)	$PGV_{m,GLS}$ (m/s)	β_{tot}
A-B	X60	1	0.715	2.099	4.086	-	0.746	0.835	2.491	4.898	-	0.703
A-B	X65	1	0.858	2.788	-	-	0.706	0.938	2.962	-	-	0.702
A-B	X70	1	1.018	3.659	-	-	0.669	1.173	4.253	-	-	0.635
A-B	X60	2	1.157	4.600	-	-	0.636	1.303	-	-	-	0.637
A-B	X65	2	1.431	-	-	-	0.612	1.685	-	-	-	0.603
A-B	X70	2	2.235	-	-	-	0.593	1.933	-	-	-	0.595
A-C	X60	1	0.572	1.499	2.722	4.014	0.799	0.623	1.620	2.926	4.301	0.778
A-C	X65	1	0.656	1.852	3.520	-	0.777	0.717	2.019	3.828	-	0.749
A-C	X70	1	0.770	2.393	4.824	-	0.726	0.833	2.560	-	-	0.691
A-C	X60	2	0.899	3.139	-	-	0.659	0.995	3.523	-	-	0.644
A-C	X65	2	1.121	4.436	-	-	0.624	1.257	-	-	-	0.608
A-C	X70	2	1.370	-	-	-	0.595	1.461	-	-	-	0.597
B-C	X60	1	1.596	-	-	-	0.714	1.674	-	-	-	0.703
B-C	X65	1	1.628	-	-	-	0.720	1.963	-	-	-	0.687
B-C	X70	1	2.020	-	-	-	0.668	2.214	-	-	-	0.669
B-C	X60	2	3.177	-	-	-	0.615	3.119	-	-	-	0.609
B-C	X65	2	3.552	-	-	-	0.603	3.728	-	-	-	0.577
B-C	X70	2	4.083	-	-	-	0.588	4.199	-	-	-	0.575
Soil	Steel Grade	h (m)	Cohesive soil deposit – Trench type TB					Cohesionless soil deposit – Trench type TB				
			$PGV_{m,OLS}$ (m/s)	$PGV_{m,PILS}$ (m/s)	$PGV_{m,ULS}$ (m/s)	$PGV_{m,GLS}$ (m/s)	β_{tot}	$PGV_{m,OLS}$ (m/s)	$PGV_{m,PILS}$ (m/s)	$PGV_{m,ULS}$ (m/s)	$PGV_{m,GLS}$ (m/s)	β_{tot}
A-B	X60	1	0.289	0.560	0.842	1.098	1.092	0.334	0.649	0.979	1.280	1.078
A-B	X65	1	0.305	0.603	0.919	1.209	1.115	0.354	0.704	1.078	1.424	1.095
A-B	X70	1	0.329	0.676	1.055	1.410	1.105	0.378	0.782	1.226	1.643	1.079
A-B	X60	2	0.308	0.615	0.943	1.246	1.158	0.359	0.741	1.160	1.554	1.105
A-B	X65	2	0.339	0.714	1.132	1.528	1.146	0.402	0.890	1.454	2.003	1.088
A-B	X70	2	0.374	0.837	1.376	1.903	1.120	0.448	1.060	1.804	2.552	1.029
A-C	X60	1	0.259	0.474	0.689	0.879	1.143	0.283	0.511	0.736	0.934	1.140
A-C	X65	1	0.272	0.507	0.745	0.958	1.169	0.297	0.546	0.796	1.017	1.180
A-C	X70	1	0.288	0.549	0.819	1.064	1.179	0.311	0.581	0.856	1.102	1.194
A-C	X60	2	0.266	0.486	0.706	0.900	1.267	0.295	0.552	0.814	1.048	1.233
A-C	X65	2	0.303	0.600	0.915	1.206	1.232	0.334	0.673	1.039	1.379	1.207
A-C	X70	2	0.320	0.652	1.014	1.352	1.227	0.349	0.723	1.134	1.521	1.209
B-C	X60	1	0.620	1.670	3.082	4.595	0.912	0.714	1.971	3.695	-	0.887
B-C	X65	1	0.683	1.951	3.734	-	0.900	0.769	2.200	4.213	-	0.881
B-C	X70	1	0.781	2.419	4.866	-	0.857	0.813	2.384	4.639	-	0.883
B-C	X60	2	0.749	2.311	4.638	-	0.864	0.817	2.489	4.957	-	0.879
B-C	X65	2	0.887	3.023	-	-	0.840	1.174	4.521	-	-	0.786
B-C	X70	2	1.088	4.200	-	-	0.783	1.337	-	-	-	0.741

Table A10. Median peak ground velocity corresponding to the limit states, $PGV_{m,i}$, and total lognormal standard deviation, β_{tot} , for 914.4 mm pipelines embedded in soil deposit of depth $H = 30$ m (- : the limit state is not reached).

Soil	Steel Grade	Burial depth, h (m)	Cohesive soil deposit – Trench type TA					Cohesionless soil deposit – Trench type TA				
			$PGV_{m,OLS}$ (m/s)	$PGV_{m,PILS}$ (m/s)	$PGV_{m,ULS}$ (m/s)	$PGV_{m,GLS}$ (m/s)	β_{tot}	$PGV_{m,OLS}$ (m/s)	$PGV_{m,PILS}$ (m/s)	$PGV_{m,ULS}$ (m/s)	$PGV_{m,GLS}$ (m/s)	β_{tot}
A-B	X60	1	0.736	2.160	4.205	-	0.879	0.826	2.563	-	-	0.850
A-B	X65	1	0.922	3.101	-	-	0.807	1.042	3.716	-	-	0.779
A-B	X70	1	1.081	4.021	-	-	0.761	1.228	4.858	-	-	0.735
A-B	X60	2	0.945	3.426	-	-	0.816	1.009	3.729	-	-	0.833
A-B	X65	2	1.286	-	-	-	0.720	2.073	-	-	-	0.556
A-B	X70	2	1.336	-	-	-	0.733	1.536	-	-	-	0.723
A-C	X60	1	0.763	2.411	4.912	-	0.861	0.796	2.546	-	-	0.836
A-C	X65	1	1.203	-	-	-	0.755	1.011	3.740	-	-	0.763
A-C	X70	1	1.079	4.184	-	-	0.768	1.323	-	-	-	0.755
A-C	X60	2	0.927	3.460	-	-	0.840	1.958	-	-	-	0.541
A-C	X65	2	1.832	-	-	-	0.625	1.268	-	-	-	0.745
A-C	X70	2	1.437	-	-	-	0.723	1.519	-	-	-	0.717
B-C	X60	1	3.185	-	-	-	0.545	2.905	-	-	-	0.736
B-C	X65	1	2.974	-	-	-	0.702	4.900	-	-	-	0.697
B-C	X70	1	3.646	-	-	-	0.678	-	-	-	-	0.669
B-C	X60	2	2.819	-	-	-	0.705	-	-	-	-	0.688
B-C	X65	2	4.159	-	-	-	0.655	-	-	-	-	0.646
B-C	X70	2	-	-	-	-	-	-	-	-	-	-
Soil	Steel Grade	h (m)	Cohesive soil deposit – Trench type TB					Cohesionless soil deposit – Trench type TB				
			$PGV_{m,OLS}$ (m/s)	$PGV_{m,PILS}$ (m/s)	$PGV_{m,ULS}$ (m/s)	$PGV_{m,GLS}$ (m/s)	β_{tot}	$PGV_{m,OLS}$ (m/s)	$PGV_{m,PILS}$ (m/s)	$PGV_{m,ULS}$ (m/s)	$PGV_{m,GLS}$ (m/s)	β_{tot}
A-B	X60	1	0.351	0.738	1.169	1.836	1.148	0.376	0.813	1.310	2.091	1.173
A-B	X65	1	0.401	0.900	1.484	2.424	1.101	0.427	0.983	1.646	2.728	1.110
A-B	X70	1	0.440	1.045	1.783	3.011	1.090	0.480	1.193	2.095	3.637	1.056
A-B	X60	2	0.357	0.769	1.234	1.963	1.233	0.391	0.894	1.491	2.461	1.200
A-B	X65	2	0.409	0.946	1.589	2.641	1.166	0.427	1.004	1.702	2.856	1.178
A-B	X70	2	0.614	1.954	4.000	-	0.870	0.587	1.758	3.463	-	0.951
A-C	X60	1	0.333	0.709	1.131	1.787	1.155	0.337	0.706	1.115	1.745	1.198
A-C	X65	1	0.374	0.836	1.373	2.235	1.138	0.383	0.852	1.397	2.269	1.144
A-C	X70	1	0.432	1.067	1.866	3.229	1.066	0.451	1.134	2.007	3.511	1.040
A-C	X60	2	0.347	0.773	1.269	2.063	1.221	0.347	0.773	1.269	2.063	1.221
A-C	X65	2	0.384	0.885	1.483	2.460	1.210	0.392	0.911	1.536	2.563	1.197
A-C	X70	2	0.546	1.669	3.329	-	0.950	0.553	1.693	3.383	-	0.938
B-C	X60	1	0.852	2.614	-	-	0.955	0.858	2.628	-	-	0.916
B-C	X65	1	0.927	2.959	-	-	0.894	1.200	4.450	-	-	0.838
B-C	X70	1	1.131	4.130	-	-	0.823	1.475	-	-	-	0.769
B-C	X60	2	0.993	3.549	-	-	0.877	1.067	3.870	-	-	0.888
B-C	X65	2	0.962	3.222	-	-	0.907	1.385	-	-	-	0.798
B-C	X70	2	1.571	-	-	-	0.710	1.884	-	-	-	0.708

Table A11. Median peak ground velocity corresponding to the limit states, $PGV_{m,i}$, and total lognormal standard deviation, β_{tot} , for 914.4 mm pipelines embedded in soil deposit of depth $H = 60$ m (- : the limit state is not reached).

Soil	Steel Grade	Burial depth, h (m)	Cohesive soil deposit – Trench type TA					Cohesionless soil deposit – Trench type TA				
			$PGV_{m,OLS}$ (m/s)	$PGV_{m,PILS}$ (m/s)	$PGV_{m,ULS}$ (m/s)	$PGV_{m,GLS}$ (m/s)	β_{tot}	$PGV_{m,OLS}$ (m/s)	$PGV_{m,PILS}$ (m/s)	$PGV_{m,ULS}$ (m/s)	$PGV_{m,GLS}$ (m/s)	β_{tot}
A-B	X60	1	0.742	2.112	4.032	-	0.880	0.661	2.004	3.981	-	0.850
A-B	X65	1	0.695	2.216	4.539	-	0.813	0.794	2.657	-	-	0.791
A-B	X70	1	0.806	2.818	-	-	0.769	0.892	3.183	-	-	0.770
A-B	X60	2	0.676	2.229	4.664	-	0.858	0.776	2.736	-	-	0.833
A-B	X65	2	0.882	3.387	-	-	0.770	1.050	4.422	-	-	0.743
A-B	X70	2	1.130	-	-	-	0.688	1.184	-	-	-	0.738
A-C	X60	1	0.508	1.342	2.447	4.410	0.881	0.542	1.463	2.705	4.938	0.880
A-C	X65	1	0.614	1.807	3.523	-	0.821	0.652	1.954	3.854	-	0.830
A-C	X70	1	0.693	2.198	4.489	-	0.785	0.765	2.545	-	-	0.784
A-C	X60	2	0.600	1.828	3.641	-	0.865	0.645	2.048	4.186	-	0.866
A-C	X65	2	0.767	2.688	-	-	0.780	0.837	3.104	-	-	0.784
A-C	X70	2	0.965	3.951	-	-	0.692	1.028	4.363	-	-	0.705
B-C	X60	1	1.294	-	-	-	0.788	1.226	4.432	-	-	0.808
B-C	X65	1	1.284	4.833	-	-	0.773	1.797	-	-	-	0.759
B-C	X70	1	1.440	-	-	-	0.741	2.143	-	-	-	0.700
B-C	X60	2	1.264	4.968	-	-	0.767	1.791	-	-	-	0.741
B-C	X65	2	1.541	-	-	-	0.721	2.461	-	-	-	0.675
B-C	X70	2	2.094	-	-	-	0.651	2.962	-	-	-	0.646
Soil	Steel Grade	h (m)	Cohesive soil deposit – Trench type TB					Cohesionless soil deposit – Trench type TB				
			$PGV_{m,OLS}$ (m/s)	$PGV_{m,PILS}$ (m/s)	$PGV_{m,ULS}$ (m/s)	$PGV_{m,GLS}$ (m/s)	β_{tot}	$PGV_{m,OLS}$ (m/s)	$PGV_{m,PILS}$ (m/s)	$PGV_{m,ULS}$ (m/s)	$PGV_{m,GLS}$ (m/s)	β_{tot}
A-B	X60	1	0.268	0.523	0.790	1.185	1.103	0.290	0.569	0.862	1.296	1.101
A-B	X65	1	0.296	0.595	0.917	1.400	1.083	0.328	0.680	1.068	1.663	1.048
A-B	X70	1	0.333	0.728	1.180	1.895	1.015	0.378	0.871	1.459	2.418	0.968
A-B	X60	2	0.278	0.567	0.879	1.353	1.154	0.313	0.683	1.105	1.772	1.093
A-B	X65	2	0.302	0.621	0.971	1.503	1.162	0.330	0.705	1.126	1.782	1.134
A-B	X70	2	0.409	1.073	1.947	3.494	0.927	0.465	1.158	2.035	3.535	0.986
A-C	X60	1	0.255	0.482	0.715	1.051	1.060	0.267	0.510	0.759	1.123	1.072
A-C	X65	1	0.281	0.550	0.833	1.252	1.032	0.289	0.560	0.842	1.257	1.074
A-C	X70	1	0.300	0.602	0.926	1.412	1.064	0.324	0.676	1.066	1.665	1.011
A-C	X60	2	0.257	0.488	0.726	1.071	1.156	0.271	0.538	0.821	1.244	1.127
A-C	X65	2	0.286	0.569	0.871	1.321	1.121	0.294	0.589	0.905	1.379	1.148
A-C	X70	2	0.378	0.943	1.660	2.887	0.882	0.376	0.920	1.599	2.749	0.931
B-C	X60	1	0.477	1.138	1.948	3.299	1.111	0.520	1.284	2.244	3.878	1.056
B-C	X65	1	0.556	1.408	2.500	4.389	1.044	0.636	1.756	3.289	-	0.976
B-C	X70	1	0.665	1.960	3.825	-	0.924	0.767	2.403	4.872	-	0.909
B-C	X60	2	0.538	1.445	2.664	4.852	1.056	0.584	1.605	2.998	-	1.059
B-C	X65	2	0.549	1.427	2.576	4.595	1.082	0.625	1.729	3.242	-	1.039
B-C	X70	2	0.885	3.293	-	-	0.828	1.019	4.060	-	-	0.793

Table A12. Median peak ground velocity corresponding to the limit states, $PGV_{m,i}$, and total lognormal standard deviation, β_{tot} , for 914.4 mm pipelines embedded in soil deposit of depth $H = 120$ m (- : the limit state is not reached).

Soil	Steel Grade	Burial depth, h (m)	Cohesive soil deposit – Trench type TA					Cohesionless soil deposit – Trench type TA				
			$PGV_{m,OLS}$ (m/s)	$PGV_{m,PILS}$ (m/s)	$PGV_{m,ULS}$ (m/s)	$PGV_{m,GLS}$ (m/s)	β_{tot}	$PGV_{m,OLS}$ (m/s)	$PGV_{m,PILS}$ (m/s)	$PGV_{m,ULS}$ (m/s)	$PGV_{m,GLS}$ (m/s)	β_{tot}
A-B	X60	1	0.428	1.130	2.061	3.713	0.889	0.508	1.382	2.567	4.708	0.852
A-B	X65	1	0.517	1.518	2.953	-	0.824	0.508	1.382	2.567	4.708	0.839
A-B	X70	1	0.615	2.013	4.191	-	0.768	0.710	2.350	4.927	-	0.731
A-B	X60	2	0.518	1.604	3.229	-	0.863	0.611	1.979	4.091	-	0.827
A-B	X65	2	0.706	2.642	-	-	0.741	0.611	1.979	4.091	-	0.827
A-B	X70	2	0.835	3.447	-	-	0.714	0.968	4.122	-	-	0.702
A-C	X60	1	0.366	0.881	1.517	2.582	0.920	0.405	0.978	1.688	2.881	0.903
A-C	X65	1	0.614	1.807	3.523	-	0.821	0.652	1.954	3.854	-	0.830
A-C	X70	1	0.493	1.413	2.711	-	0.815	0.547	1.576	3.033	-	0.790
A-C	X60	2	0.418	1.124	2.072	3.773	0.917	0.468	1.298	2.438	4.522	0.889
A-C	X65	2	0.767	2.688	-	-	0.780	0.470	1.311	2.473	4.606	0.890
A-C	X70	2	0.687	2.534	-	-	0.714	0.764	2.897	-	-	0.699
B-C	X60	1	0.934	3.451	-	-	0.799	1.005	3.680	-	-	0.787
B-C	X65	1	1.104	4.455	-	-	0.753	1.318	-	-	-	0.736
B-C	X70	1	1.267	-	-	-	0.717	1.552	-	-	-	0.709
B-C	X60	2	1.090	4.631	-	-	0.777	1.275	-	-	-	0.774
B-C	X65	2	1.380	-	-	-	0.720	1.731	-	-	-	0.656
B-C	X70	2	1.713	-	-	-	0.695	2.139	-	-	-	0.662
Soil	Steel Grade	h (m)	Cohesive soil deposit – Trench type TB					Cohesionless soil deposit – Trench type TB				
			$PGV_{m,OLS}$ (m/s)	$PGV_{m,PILS}$ (m/s)	$PGV_{m,ULS}$ (m/s)	$PGV_{m,GLS}$ (m/s)	β_{tot}	$PGV_{m,OLS}$ (m/s)	$PGV_{m,PILS}$ (m/s)	$PGV_{m,ULS}$ (m/s)	$PGV_{m,GLS}$ (m/s)	β_{tot}
A-B	X60	1	0.206	0.374	0.540	0.775	1.223	0.235	0.424	0.609	0.870	1.229
A-B	X65	1	0.225	0.419	0.616	0.899	1.194	0.258	0.481	0.708	1.032	1.198
A-B	X70	1	0.252	0.504	0.775	1.181	1.132	0.287	0.576	0.885	1.348	1.124
A-B	X60	2	0.218	0.417	0.624	0.926	1.268	0.242	0.458	0.680	1.000	1.267
A-B	X65	2	0.225	0.417	0.609	0.884	1.297	0.256	0.481	0.709	1.037	1.268
A-B	X70	2	0.310	0.747	1.286	2.190	1.039	0.335	0.784	1.327	2.222	1.023
A-C	X60	1	0.193	0.340	0.482	0.678	1.245	0.212	0.369	0.520	0.728	1.245
A-C	X65	1	0.210	0.379	0.546	0.781	1.224	0.231	0.416	0.599	0.855	1.210
A-C	X70	1	0.236	0.460	0.694	1.039	1.150	0.256	0.486	0.724	1.069	1.158
A-C	X60	2	0.209	0.404	0.608	0.906	1.214	0.223	0.421	0.624	0.916	1.245
A-C	X65	2	0.211	0.378	0.543	0.774	1.333	0.228	0.409	0.587	0.837	1.328
A-C	X70	2	0.279	0.627	1.036	1.693	1.065	0.305	0.697	1.162	1.917	1.015
B-C	X60	1	0.353	0.813	1.360	2.254	1.111	0.428	1.072	1.891	3.297	1.008
B-C	X65	1	0.418	1.053	1.865	3.265	1.034	0.519	1.447	2.727	-	0.927
B-C	X70	1	0.494	1.397	2.657	4.987	0.972	0.616	1.939	3.938	-	0.866
B-C	X60	2	0.371	0.886	1.519	2.576	1.168	0.452	1.204	2.207	3.994	1.063
B-C	X65	2	0.434	1.134	2.054	3.676	1.087	0.540	1.581	3.070	-	0.956
B-C	X70	2	0.636	2.209	4.773	-	0.866	0.757	2.864	-	-	0.788

Table A13 Median peak ground velocity corresponding to the limit states, $PGV_{m,i}$, and total lognormal standard deviation, β_{tot} , for 1066.4 mm pipelines embedded in soil deposit of depth $H = 30$ m (- : the limit state is not reached).

Soil	Steel Grade	Burial depth, h (m)	Cohesive soil deposit – Trench type TA					Cohesionless soil deposit – Trench type TA				
			$PGV_{m,OLS}$ (m/s)	$PGV_{m,PILS}$ (m/s)	$PGV_{m,ULS}$ (m/s)	$PGV_{m,GLS}$ (m/s)	β_{tot}	$PGV_{m,OLS}$ (m/s)	$PGV_{m,PILS}$ (m/s)	$PGV_{m,ULS}$ (m/s)	$PGV_{m,GLS}$ (m/s)	β_{tot}
A-B	X60	1	0.995	3.221	-	-	0.819	1.135	3.905	-	-	0.801
A-B	X65	1	1.204	4.340	-	-	0.770	1.400	-	-	-	0.751
A-B	X70	1	1.366	-	-	-	0.735	1.502	-	-	-	0.734
A-B	X60	2	1.495	-	-	-	0.715	1.748	-	-	-	0.704
A-B	X65	2	2.000	-	-	-	0.658	2.333	-	-	-	0.650
A-B	X70	2	2.517	-	-	-	0.548	2.772	-	-	-	0.624
A-C	X60	1	1.063	3.761	-	-	0.793	1.108	3.958	-	-	0.786
A-C	X65	1	1.325	-	-	-	0.741	1.355	-	-	-	0.742
A-C	X70	1	1.457	-	-	-	0.727	1.508	-	-	-	0.721
A-C	X60	2	1.601	-	-	-	0.705	1.709	-	-	-	0.680
A-C	X65	2	2.128	-	-	-	0.651	2.293	-	-	-	0.631
A-C	X70	2	2.692	-	-	-	0.617	2.862	-	-	-	0.613
B-C	X60	1	4.547	-	-	-	0.700	4.427	-	-	-	0.704
B-C	X65	1	4.592	-	-	-	0.674	-	-	-	-	-
B-C	X70	1	-	-	-	-	0.661	-	-	-	-	-
B-C	X60	2	4.920	-	-	-	0.663	-	-	-	-	-
B-C	X65	2	-	-	-	-	-	-	-	-	-	-
B-C	X70	2	-	-	-	-	-	-	-	-	-	-
Soil	Steel Grade	h (m)	Cohesive soil deposit – Trench type TB					Cohesionless soil deposit – Trench type TB				
			$PGV_{m,OLS}$ (m/s)	$PGV_{m,PILS}$ (m/s)	$PGV_{m,ULS}$ (m/s)	$PGV_{m,GLS}$ (m/s)	β_{tot}	$PGV_{m,OLS}$ (m/s)	$PGV_{m,PILS}$ (m/s)	$PGV_{m,ULS}$ (m/s)	$PGV_{m,GLS}$ (m/s)	β_{tot}
A-B	X60	1	0.421	0.917	1.484	2.291	1.139	0.452	1.013	1.667	2.615	1.128
A-B	X65	1	0.457	1.027	1.695	2.666	1.151	0.507	1.204	2.057	3.336	1.096
A-B	X70	1	0.543	1.382	2.462	4.147	1.027	0.623	1.717	3.214	-	0.942
A-B	X60	2	0.448	1.025	1.711	2.717	1.152	0.507	1.259	2.208	3.668	1.083
A-B	X65	2	0.587	1.615	3.020	-	0.998	0.589	1.591	2.941	-	1.039
A-B	X70	2	0.682	2.043	4.027	-	0.960	0.810	2.706	-	-	0.871
A-C	X60	1	0.410	0.920	1.515	2.378	1.125	0.428	0.975	1.622	2.569	1.095
A-C	X65	1	0.461	1.100	1.884	3.061	1.101	0.482	1.171	2.027	3.327	1.068
A-C	X70	1	0.540	1.440	2.641	4.566	1.005	0.570	1.557	2.899	-	0.962
A-C	X60	2	0.456	1.116	1.943	3.204	1.100	0.480	1.218	2.166	3.644	1.048
A-C	X65	2	0.538	1.453	2.687	4.679	1.058	0.566	1.583	2.989	-	1.014
A-C	X70	2	0.733	2.446	-	-	0.894	0.744	2.492	-	-	0.900
B-C	X60	1	1.200	4.137	-	-	0.877	1.264	4.476	-	-	0.812
B-C	X65	1	1.253	4.409	-	-	0.843	1.773	-	-	-	0.771
B-C	X70	1	1.428	-	-	-	0.823	2.105	-	-	-	0.720
B-C	X60	2	1.145	3.920	-	-	0.876	1.798	-	-	-	0.750
B-C	X65	2	1.603	-	-	-	0.786	2.303	-	-	-	0.703
B-C	X70	2	1.956	-	-	-	0.769	3.092	-	-	-	0.673

Table A14 Median peak ground velocity corresponding to the limit states, $PGV_{m,i}$, and total lognormal standard deviation, β_{tot} , for 1066.4 mm pipelines embedded in soil deposit of depth $H = 60$ m (- : the limit state is not reached).

Soil	Steel Grade	Burial depth, h (m)	Cohesive soil deposit – Trench type TA					Cohesionless soil deposit – Trench type TA				
			$PGV_{m,OLS}$ (m/s)	$PGV_{m,PILS}$ (m/s)	$PGV_{m,ULS}$ (m/s)	$PGV_{m,GLS}$ (m/s)	β_{tot}	$PGV_{m,OLS}$ (m/s)	$PGV_{m,PILS}$ (m/s)	$PGV_{m,ULS}$ (m/s)	$PGV_{m,GLS}$ (m/s)	β_{tot}
A-B	X60	1	0.772	2.437	4.961	-	0.809	0.807	2.482	4.972	-	0.836
A-B	X65	1	0.938	3.295	-	-	0.762	0.979	3.357	-	-	0.793
A-B	X70	1	1.144	4.558	-	-	0.702	1.342	-	-	-	0.697
A-B	X60	2	1.059	4.189	-	-	0.736	1.239	-	-	-	0.722
A-B	X65	2	1.373	-	-	-	0.677	1.694	-	-	-	0.661
A-B	X70	2	1.720	-	-	-	0.633	2.053	-	-	-	0.629
A-C	X60	1	0.679	1.990	3.870	-	0.813	0.714	2.110	4.123	-	0.827
A-C	X65	1	0.819	2.662	-	-	0.760	0.867	2.857	-	-	0.768
A-C	X70	1	0.994	3.652	-	-	0.706	1.016	3.693	-	-	0.719
A-C	X60	2	0.900	3.221	-	-	0.747	0.991	3.763	-	-	0.748
A-C	X65	2	1.163	4.837	-	-	0.684	1.278	-	-	-	0.676
A-C	X70	2	1.396	-	-	-	0.645	1.538	-	-	-	0.647
B-C	X60	1	1.666	-	-	-	0.758	1.686	-	-	-	0.765
B-C	X65	1	1.770	-	-	-	0.720	2.471	-	-	-	0.725
B-C	X70	1	2.114	-	-	-	0.683	3.021	-	-	-	0.665
B-C	X60	2	2.362	-	-	-	0.682	2.749	-	-	-	0.688
B-C	X65	2	3.285	-	-	-	0.637	3.754	-	-	-	0.641
B-C	X70	2	3.977	-	-	-	0.618	4.534	-	-	-	0.624
Soil	Steel Grade	h (m)	Cohesive soil deposit – Trench type TB					Cohesionless soil deposit – Trench type TB				
			$PGV_{m,OLS}$ (m/s)	$PGV_{m,PILS}$ (m/s)	$PGV_{m,ULS}$ (m/s)	$PGV_{m,GLS}$ (m/s)	β_{tot}	$PGV_{m,OLS}$ (m/s)	$PGV_{m,PILS}$ (m/s)	$PGV_{m,ULS}$ (m/s)	$PGV_{m,GLS}$ (m/s)	β_{tot}
A-B	X60	1	0.317	0.635	0.977	1.440	1.104	0.365	0.783	1.255	1.921	1.016
A-B	X65	1	0.349	0.734	1.161	1.757	1.088	0.452	1.086	1.870	3.053	0.994
A-B	X70	1	0.405	0.945	1.595	2.560	1.011	0.623	1.717	3.214	-	0.942
A-B	X60	2	0.345	0.738	1.182	1.808	1.090	0.395	0.913	1.531	2.444	1.009
A-B	X65	2	0.399	0.927	1.562	2.501	1.050	0.477	1.234	2.222	3.777	0.947
A-B	X70	2	0.518	1.436	2.697	4.766	0.931	0.594	1.565	2.849	4.892	0.958
A-C	X60	1	0.290	0.546	0.808	1.150	1.137	0.312	0.607	0.916	1.329	1.100
A-C	X65	1	0.316	0.617	0.934	1.357	1.118	0.342	0.692	1.071	1.589	1.086
A-C	X70	1	0.363	0.782	1.258	1.933	1.009	0.406	0.932	1.560	2.482	0.951
A-C	X60	2	0.310	0.615	0.938	1.374	1.141	0.334	0.699	1.103	1.665	1.080
A-C	X65	2	0.373	0.833	1.369	2.144	1.025	0.567	1.584	2.991	-	1.014
A-C	X70	2	0.454	1.148	2.039	3.426	0.972	0.526	1.489	2.832	-	0.884
B-C	X60	1	0.622	1.620	2.928	4.997	1.018	0.659	1.728	3.136	-	0.981
B-C	X65	1	0.695	1.922	3.605	-	0.978	0.808	2.377	4.634	-	0.943
B-C	X70	1	0.809	2.463	4.904	-	0.931	0.864	2.628	-	-	0.927
B-C	X60	2	0.667	1.846	3.467	-	0.998	0.802	2.443	4.866	-	0.930
B-C	X65	2	0.843	2.688	-	-	0.922	0.954	3.199	-	-	0.895
B-C	X70	2	1.078	3.989	-	-	0.854	1.313	-	-	-	0.788

Table A15 Median peak ground velocity corresponding to the limit states, $PGV_{m,i}$, and total lognormal standard deviation, β_{tot} , for 1066.4 mm pipelines embedded in soil deposit of depth $H = 120$ m (- : the limit state is not reached).

Soil	Steel Grade	Burial depth, h (m)	Cohesive soil deposit – Trench type TA					Cohesionless soil deposit – Trench type TA				
			$PGV_{m,OLS}$ (m/s)	$PGV_{m,PILS}$ (m/s)	$PGV_{m,ULS}$ (m/s)	$PGV_{m,GLS}$ (m/s)	β_{tot}	$PGV_{m,OLS}$ (m/s)	$PGV_{m,PILS}$ (m/s)	$PGV_{m,ULS}$ (m/s)	$PGV_{m,GLS}$ (m/s)	β_{tot}
A-B	X60	1	0.575	1.675	3.244	-	0.823	0.667	1.970	3.849	-	0.787
A-B	X65	1	0.699	2.271	4.705	-	0.772	0.821	2.728	-	-	0.705
A-B	X70	1	0.877	3.296	-	-	0.700	1.013	3.848	-	-	0.660
A-B	X60	2	0.828	3.151	-	-	0.728	0.950	3.681	-	-	0.715
A-B	X65	2	1.113	-	-	-	0.659	1.275	-	-	-	0.653
A-B	X70	2	1.389	-	-	-	0.620	1.619	-	-	-	0.613
A-C	X60	1	0.488	1.312	2.420	4.207	0.842	0.534	1.425	2.616	4.526	0.830
A-C	X65	1	0.583	1.726	3.377	-	0.790	0.636	1.869	3.640	-	0.752
A-C	X70	1	0.697	2.308	4.840	-	0.734	0.772	2.567	-	-	0.687
A-C	X60	2	0.631	2.038	4.208	-	0.768	0.701	2.309	4.825	-	0.754
A-C	X65	2	0.834	3.174	-	-	0.696	0.923	3.579	-	-	0.666
A-C	X70	2	1.033	4.498	-	-	0.647	1.149	-	-	-	0.640
B-C	X60	1	1.322	-	-	-	0.752	1.349	-	-	-	0.743
B-C	X65	1	1.459	-	-	-	0.734	1.594	-	-	-	0.734
B-C	X70	1	1.744	-	-	-	0.701	2.050	-	-	-	0.681
B-C	X60	2	2.025	-	-	-	0.669	2.137	-	-	-	0.686
B-C	X65	2	2.832	-	-	-	0.622	2.850	-	-	-	0.618
B-C	X70	2	3.488	-	-	-	0.600	3.255	-	-	-	0.621
Soil	Steel Grade	h (m)	Cohesive soil deposit – Trench type TB					Cohesionless soil deposit – Trench type TB				
			$PGV_{m,OLS}$ (m/s)	$PGV_{m,PILS}$ (m/s)	$PGV_{m,ULS}$ (m/s)	$PGV_{m,GLS}$ (m/s)	β_{tot}	$PGV_{m,OLS}$ (m/s)	$PGV_{m,PILS}$ (m/s)	$PGV_{m,ULS}$ (m/s)	$PGV_{m,GLS}$ (m/s)	β_{tot}
A-B	X60	1	0.243	0.457	0.674	0.958	1.189	0.282	0.535	0.796	1.138	1.164
A-B	X65	1	0.265	0.514	0.775	1.122	1.185	0.265	0.514	0.775	1.122	1.185
A-B	X70	1	0.299	0.631	1.002	1.521	1.106	0.342	0.722	1.147	1.742	1.073
A-B	X60	2	0.255	0.492	0.738	1.065	1.210	0.296	0.593	0.910	1.340	1.164
A-B	X65	2	0.290	0.599	0.937	1.405	1.188	0.290	0.599	0.939	1.407	1.189
A-B	X70	2	0.356	0.841	1.431	2.312	1.073	0.419	1.041	1.828	3.040	0.990
A-C	X60	1	0.221	0.396	0.567	0.785	1.230	0.245	0.437	0.625	0.864	1.217
A-C	X65	1	0.239	0.441	0.643	0.905	1.239	0.263	0.479	0.695	0.973	1.233
A-C	X70	1	0.267	0.526	0.800	1.169	1.168	0.284	0.542	0.809	1.161	1.190
A-C	X60	2	0.231	0.422	0.611	0.855	1.269	0.251	0.461	0.672	0.943	1.266
A-C	X65	2	0.272	0.548	0.845	1.251	1.208	0.301	0.622	0.974	1.460	1.173
A-C	X70	2	0.314	0.686	1.113	1.723	1.162	0.339	0.746	1.216	1.889	1.138
B-C	X60	1	0.482	1.262	2.288	3.915	0.976	0.578	1.619	3.060	-	0.890
B-C	X65	1	0.554	1.556	2.948	-	0.953	0.692	2.134	4.281	-	0.866
B-C	X70	1	0.646	2.005	4.041	-	0.898	0.873	3.164	-	-	0.777
B-C	X60	2	0.541	1.542	2.948	-	0.955	0.706	2.317	4.831	-	0.847
B-C	X65	2	0.681	2.225	4.629	-	0.888	0.913	3.505	-	-	0.775
B-C	X70	2	0.888	3.432	-	-	0.804	1.243	-	-	-	0.704

Table A16 Median peak ground velocity corresponding to the limit states, $PGV_{m,i}$, and total lognormal standard deviation, β_{tot} , for 1219.2 mm pipelines embedded in soil deposit of depth $H = 30$ m (- : the limit state is not reached).

Soil	Steel Grade	Burial depth, h (m)	Cohesive soil deposit – Trench type TA					Cohesionless soil deposit – Trench type TA				
			$PGV_{m,OLS}$ (m/s)	$PGV_{m,PILS}$ (m/s)	$PGV_{m,ULS}$ (m/s)	$PGV_{m,GLS}$ (m/s)	β_{tot}	$PGV_{m,OLS}$ (m/s)	$PGV_{m,PILS}$ (m/s)	$PGV_{m,ULS}$ (m/s)	$PGV_{m,GLS}$ (m/s)	β_{tot}
A-B	X60	1	1.288	4.523	-	-	0.774	1.449	-	-	-	0.775
A-B	X65	1	1.736	-	-	-	0.695	1.909	-	-	-	0.702
A-B	X70	1	2.353	-	-	-	0.667	2.217	-	-	-	0.669
A-B	X60	2	1.706	-	-	-	0.697	1.938	-	-	-	0.693
A-B	X65	2	2.100	-	-	-	0.684	2.192	-	-	-	0.697
A-B	X70	2	2.666	-	-	-	0.614	3.160	-	-	-	0.607
A-C	X60	1	1.349	-	-	-	0.771	1.401	-	-	-	0.768
A-C	X65	1	1.851	-	-	-	0.689	1.928	-	-	-	0.688
A-C	X70	1	2.176	-	-	-	0.656	2.247	-	-	-	0.657
A-C	X60	2	1.840	-	-	-	0.688	1.941	-	-	-	0.687
A-C	X65	2	2.143	-	-	-	0.691	2.270	-	-	-	0.685
A-C	X70	2	3.121	-	-	-	0.599	-	-	-	-	0.597
B-C	X60	1	-	-	-	-	-	-	-	-	-	-
B-C	X65	1	-	-	-	-	-	-	-	-	-	-
B-C	X70	1	-	-	-	-	-	-	-	-	-	-
B-C	X60	2	-	-	-	-	-	-	-	-	-	-
B-C	X65	2	-	-	-	-	-	-	-	-	-	-
B-C	X70	2	-	-	-	-	-	-	-	-	-	-
Soil	Steel Grade	h (m)	Cohesive soil deposit – Trench type TB					Cohesionless soil deposit – Trench type TB				
			$PGV_{m,OLS}$ (m/s)	$PGV_{m,PILS}$ (m/s)	$PGV_{m,ULS}$ (m/s)	$PGV_{m,GLS}$ (m/s)	β_{tot}	$PGV_{m,OLS}$ (m/s)	$PGV_{m,PILS}$ (m/s)	$PGV_{m,ULS}$ (m/s)	$PGV_{m,GLS}$ (m/s)	β_{tot}
A-B	X60	1	0.526	1.251	2.140	3.373	1.050	0.580	1.446	2.544	4.109	1.008
A-B	X65	1	0.574	1.422	2.492	4.012	1.044	0.651	1.724	3.149	-	0.978
A-B	X70	1	0.645	1.722	3.159	-	0.996	0.744	2.144	4.126	-	0.925
A-B	X60	2	0.515	1.230	2.106	3.325	1.096	0.583	1.497	2.683	4.403	1.035
A-B	X65	2	0.589	1.517	2.723	4.472	1.066	0.727	2.133	4.153	-	0.990
A-B	X70	2	0.669	1.871	3.534	-	1.019	0.799	2.493	-	-	0.919
A-C	X60	1	0.527	1.319	2.327	3.767	1.011	0.553	1.412	2.522	4.125	0.987
A-C	X65	1	0.596	1.591	2.921	4.891	0.986	0.627	1.709	3.179	-	0.949
A-C	X70	1	0.687	2.010	3.907	-	0.932	0.728	2.187	4.318	-	0.892
A-C	X60	2	0.575	1.538	2.827	4.739	1.033	0.562	1.497	2.743	4.585	0.997
A-C	X65	2	0.621	1.742	3.298	-	1.003	0.665	1.953	3.802	-	0.953
A-C	X70	2	0.735	2.311	4.694	-	0.928	0.867	3.041	-	-	0.873
B-C	X60	1	1.508	-	-	-	0.793	2.062	-	-	-	0.738
B-C	X65	1	1.962	-	-	-	0.791	2.547	-	-	-	0.701
B-C	X70	1	2.207	-	-	-	0.766	3.076	-	-	-	0.666
B-C	X60	2	1.731	-	-	-	0.796	2.316	-	-	-	0.706
B-C	X65	2	2.120	-	-	-	0.766	2.847	-	-	-	0.665
B-C	X70	2	2.192	-	-	-	0.734	3.653	-	-	-	0.621

Table A17 Median peak ground velocity corresponding to the limit states, $PGV_{m,i}$, and total lognormal standard deviation, β_{tot} , for 1219.2 mm pipelines embedded in soil deposit of depth $H = 60$ m (- : the limit state is not reached).

Soil	Steel Grade	Burial depth, h (m)	Cohesive soil deposit – Trench type TA					Cohesionless soil deposit – Trench type TA				
			$PGV_{m,OLS}$ (m/s)	$PGV_{m,PILS}$ (m/s)	$PGV_{m,ULS}$ (m/s)	$PGV_{m,GLS}$ (m/s)	β_{tot}	$PGV_{m,OLS}$ (m/s)	$PGV_{m,PILS}$ (m/s)	$PGV_{m,ULS}$ (m/s)	$PGV_{m,GLS}$ (m/s)	β_{tot}
A-B	X60	1	1.062	3.790	-	-	0.737	1.111	3.876	-	-	0.768
A-B	X65	1	1.352	-	-	-	0.681	1.369	-	-	-	0.724
A-B	X70	1	1.958	-	-	-	0.640	1.609	-	-	-	0.688
A-B	X60	2	1.342	-	-	-	0.683	1.387	-	-	-	0.722
A-B	X65	2	1.635	-	-	-	0.649	2.000	-	-	-	0.640
A-B	X70	2	2.090	-	-	-	0.604	2.486	-	-	-	0.602
A-C	X60	1	0.939	3.140	-	-	0.733	0.997	3.388	-	-	0.748
A-C	X65	1	1.106	4.041	-	-	0.696	1.201	4.524	-	-	0.694
A-C	X70	1	1.357	-	-	-	0.646	1.458	-	-	-	0.650
A-C	X60	2	1.114	4.267	-	-	0.697	1.250	-	-	-	0.697
A-C	X65	2	1.436	-	-	-	0.642	1.441	-	-	-	0.670
A-C	X70	2	1.754	-	-	-	0.610	1.857	-	-	-	0.619
B-C	X60	1	2.192	-	-	-	0.730	2.466	-	-	-	0.710
B-C	X65	1	2.562	-	-	-	0.671	3.619	-	-	-	0.677
B-C	X70	1	2.988	-	-	-	0.648	4.069	-	-	-	0.644
B-C	X60	2	2.784	-	-	-	0.664	3.435	-	-	-	0.662
B-C	X65	2	3.179	-	-	-	0.669	4.495	-	-	-	0.627
B-C	X70	2	4.364	-	-	-	0.611	-	-	-	-	-
Soil	Steel Grade	h (m)	Cohesive soil deposit – Trench type TB					Cohesionless soil deposit – Trench type TB				
			$PGV_{m,OLS}$ (m/s)	$PGV_{m,PILS}$ (m/s)	$PGV_{m,ULS}$ (m/s)	$PGV_{m,GLS}$ (m/s)	β_{tot}	$PGV_{m,OLS}$ (m/s)	$PGV_{m,PILS}$ (m/s)	$PGV_{m,ULS}$ (m/s)	$PGV_{m,GLS}$ (m/s)	β_{tot}
A-B	X60	1	0.382	0.823	1.324	1.982	1.060	0.440	1.006	1.679	2.592	1.023
A-B	X65	1	0.417	0.932	1.532	2.338	1.074	0.489	1.174	2.019	3.197	1.013
A-B	X70	1	0.469	1.132	1.950	3.095	1.035	0.551	1.426	2.568	4.232	0.987
A-B	X60	2	0.372	0.793	1.267	1.885	1.150	0.449	1.072	1.838	2.904	1.010
A-B	X65	2	0.442	1.044	1.778	2.792	1.059	0.563	1.539	2.868	4.863	0.953
A-B	X70	2	0.487	1.223	2.160	3.501	1.098	0.598	1.698	3.237	-	1.006
A-C	X60	1	0.346	0.699	1.079	1.560	1.071	0.369	0.761	1.192	1.744	1.070
A-C	X65	1	0.368	0.755	1.178	1.718	1.114	0.405	0.872	1.402	2.098	1.068
A-C	X70	1	0.415	0.923	1.513	2.300	1.056	0.449	1.034	1.731	2.680	1.052
A-C	X60	2	0.344	0.688	1.057	1.522	1.206	0.366	0.772	1.227	1.816	1.096
A-C	X65	2	0.376	0.793	1.258	1.861	1.170	0.425	0.977	1.635	2.531	1.086
A-C	X70	2	0.412	0.920	1.511	2.304	1.171	0.472	1.159	2.021	3.240	1.120
B-C	X60	1	0.824	2.424	4.724	-	0.900	0.859	2.464	4.729	-	0.938
B-C	X65	1	0.937	2.926	-	-	0.881	0.909	2.655	-	-	0.937
B-C	X70	1	0.978	3.108	-	-	0.883	1.063	3.425	-	-	0.883
B-C	X60	2	0.818	2.423	4.744	-	0.934	0.772	2.109	3.926	-	1.011
B-C	X65	2	0.972	3.179	-	-	0.894	1.037	3.356	-	-	0.904
B-C	X70	2	1.110	3.943	-	-	0.852	1.009	3.228	-	-	0.937

Table A18 Median peak ground velocity corresponding to the limit states, $PGV_{m,i}$, and total lognormal standard deviation, β_{tot} , for 1219.2 mm pipelines embedded in soil deposit of depth $H = 120$ m (- : the limit state is not reached).

Soil	Steel Grade	Burial depth, h (m)	Cohesive soil deposit – Trench type TA					Cohesionless soil deposit – Trench type TA				
			$PGV_{m,OLS}$ (m/s)	$PGV_{m,PILS}$ (m/s)	$PGV_{m,ULS}$ (m/s)	$PGV_{m,GLS}$ (m/s)	β_{tot}	$PGV_{m,OLS}$ (m/s)	$PGV_{m,PILS}$ (m/s)	$PGV_{m,ULS}$ (m/s)	$PGV_{m,GLS}$ (m/s)	β_{tot}
A-B	X60	1	0.783	2.573	-	-	0.764	0.882	2.877	-	-	0.734
A-B	X65	1	1.022	3.933	-	-	0.686	1.176	4.569	-	-	0.650
A-B	X70	1	1.464	-	-	-	0.650	1.392	-	-	-	0.620
A-B	X60	2	0.957	3.684	-	-	0.711	1.109	4.382	-	-	0.692
A-B	X65	2	1.304	-	-	-	0.641	1.421	-	-	-	0.671
A-B	X70	2	1.595	-	-	-	0.615	1.836	-	-	-	0.605
A-C	X60	1	0.664	2.030	4.050	-	0.759	0.729	2.219	4.418	-	0.732
A-C	X65	1	0.823	2.840	-	-	0.701	0.904	3.116	-	-	0.665
A-C	X70	1	0.988	3.823	-	-	0.652	1.062	4.050	-	-	0.628
A-C	X60	2	0.753	2.547	-	-	0.727	1.327	4.918	-	-	0.558
A-C	X65	2	0.988	3.923	-	-	0.670	1.128	4.667	-	-	0.629
A-C	X70	2	1.253	-	-	-	0.620	1.414	-	-	-	0.604
B-C	X60	1	1.694	-	-	-	0.736	1.764	-	-	-	0.720
B-C	X65	1	2.191	-	-	-	0.668	2.227	-	-	-	0.686
B-C	X70	1	2.571	-	-	-	0.643	2.969	-	-	-	0.633
B-C	X60	2	2.333	-	-	-	0.652	2.267	-	-	-	0.718
B-C	X65	2	2.672	-	-	-	0.662	3.071	-	-	-	0.624
B-C	X70	2	3.794	-	-	-	0.590	3.780	-	-	-	0.604
Soil	Steel Grade	h (m)	Cohesive soil deposit – Trench type TB					Cohesionless soil deposit – Trench type TB				
			$PGV_{m,OLS}$ (m/s)	$PGV_{m,PILS}$ (m/s)	$PGV_{m,ULS}$ (m/s)	$PGV_{m,GLS}$ (m/s)	β_{tot}	$PGV_{m,OLS}$ (m/s)	$PGV_{m,PILS}$ (m/s)	$PGV_{m,ULS}$ (m/s)	$PGV_{m,GLS}$ (m/s)	β_{tot}
A-B	X60	1	0.297	0.610	0.952	1.389	1.090	0.347	0.726	1.146	1.689	1.051
A-B	X65	1	0.322	0.680	1.079	1.597	1.089	0.417	0.851	1.323	1.924	1.076
A-B	X70	1	0.351	0.779	1.274	1.935	1.064	0.420	0.970	1.629	2.529	0.989
A-B	X60	2	0.291	0.588	0.910	1.318	1.153	0.340	0.715	1.133	1.675	1.091
A-B	X65	2	0.322	0.682	1.086	1.610	1.147	0.390	0.886	1.472	2.263	1.074
A-B	X70	2	0.359	0.814	1.352	2.079	1.121	0.434	1.057	1.831	2.920	1.013
A-C	X60	1	0.266	0.515	0.775	1.095	1.140	0.290	0.552	0.822	1.153	1.138
A-C	X65	1	0.282	0.551	0.833	1.183	1.164	0.306	0.587	0.879	1.239	1.158
A-C	X70	1	0.302	0.614	0.951	1.378	1.151	0.329	0.660	1.015	1.462	1.134
A-C	X60	2	0.262	0.502	0.750	1.055	1.238	0.279	0.527	0.780	1.089	1.235
A-C	X65	2	0.285	0.565	0.864	1.238	1.241	0.312	0.627	0.966	1.393	1.216
A-C	X70	2	0.314	0.661	1.048	1.548	1.203	0.339	0.714	1.131	1.672	1.208
B-C	X60	1	0.640	1.884	3.670	-	0.881	0.674	1.883	3.557	-	0.903
B-C	X65	1	0.751	2.408	4.950	-	0.832	0.788	2.402	4.787	-	0.869
B-C	X70	1	0.905	3.264	-	-	0.776	0.905	3.005	-	-	0.831
B-C	X60	2	0.669	2.065	4.147	-	0.867	0.756	2.371	4.809	-	0.876
B-C	X65	2	0.817	2.831	-	-	0.824	1.129	4.566	-	-	0.778
B-C	X70	2	1.017	4.057	-	-	0.740	1.111	4.405	-	-	0.807